Diagenetic and Burial History of the Lower Permian White Rim Sandstone in the Tar Sand Triangle, Paradox Basin, Southeastern Utah

U.S. GEOLOGICAL SURVEY BULLETIN 2000–I

On the Front Cover. View south toward the LaSal Mountains along the Colorado River between Cisco and Moab, Utah. Fisher Towers in center is composed of Permian Cutler Formation and capped by Triassic Moenkopi Formation. The prominent mesa at left center is capped by Jurassic Kayenta Formation and Wingate Sandstone and underlain by slope-forming Triassic Chinle and Moenkopi Formations. The Chinle-Moenkopi contact is marked by a thin white ledge-forming gritstone. The valley between Fisher Towers and Fisher Mesa in the background is part of Richardson Mesa, part of Professor Valley. Photograph by Omer B. Raup, U.S. Geological Survey.

DIAGENETIC AND BURIAL HISTORY OF THE LOWER PERMIAN WHITE RIM SANDSTONE IN THE TAR SAND TRIANGLE, PARADOX BASIN, SOUTHEASTERN UTAH

Frontispiece. Lower Permian White Rim Sandstone rimming the top of "Turk's head" along the Green River in Canyonlands National Park, southeastern Utah.

Diagenetic and Burial History of the Lower Permian White Rim Sandstone in the Tar Sand Triangle, Paradox Basin, Southeastern Utah

By Paula L. Hansley

EVOLUTION OF SEDIMENTARY BASINS—PARADOX BASIN
A.C. Huffman, Jr., Project Coordinator

U.S. GEOLOGICAL SURVEY BULLETIN 2000–I

A multidisciplinary approach to research studies of sedimentary rocks and their constituents and the evolution of sedimentary basins, both ancient and modern

UNITED STATES GOVERNMENT PRINTING OFFICE, WASHINGTON : 1995

U.S. DEPARTMENT OF THE INTERIOR
BRUCE BABBITT, Secretary

U.S. GEOLOGICAL SURVEY
Gordon P. Eaton, Director

Published in the Central Region, Denver, Colorado
Manuscript approved for publication February 1, 1995
Edited by Judith Stoeser
Photocomposition and graphics by Norma J. Maes

For sale by U.S. Geological Survey, Information Services
Box 25286, Federal Center
Denver, CO 80225

Library of Congress Cataloging-in-Publication Data

Hansley, Paula L.
Diagenetic and burial history of the Lower Permian White Rim Sandstone in the Tar Sand Triangle, Paradox Basin, southeastern Utah / by Paula L. Hansley.
p. cm. — (Evolution of sedimentary basins — Paradox basin ; I)
(U.S. Geological Survey bulletin ; 2000)
Includes bibliographical references.
Supt. of Docs. no.: I 19.3:2000–I
1. Sandstone—Utah. 2. Diagenesis—Utah. 3. Geology, Stratigraphic—Permian. 4. Petroleum—Geology—Utah. 5. White Rim Sandstone (Utah) I. Title. II. Series. III. Series: Evolution of sedimentary basins—Paradox Basin ; ch. I.
QE75.B9 no. 2000–I
[QE471.15.S25]
557.3 s—dc20
[552′.5′09792] 95–9915
CIP

CONTENTS

FIGURES

TABLES

Diagenetic and Burial History of the Lower Permian White Rim Sandstone in the Tar Sand Triangle, Paradox Basin, Southeastern Utah

By Paula L. Hansley

ABSTRACT

Subsurface petrologic study and burial history reconstruction of the Lower Permian White Rim Sandstone in the Tar Sand triangle on the western edge of the Paradox Basin in southeastern Utah suggest that oil migrated into White Rim reservoirs after significant burial during the early Tertiary. Primary(?) oil-bearing and hydrous, two-phase inclusions that have homogenization temperatures averaging 83°C (minimum temperature of formation) are present in growth zones in authigenic dolomite. Although this temperature is close to the temperature (85°–90°C) of the White Rim at maximum burial in Cretaceous to middle Tertiary time, it may not reflect depth of burial because dolomite may have precipitated from warm oil-bearing brines that migrated upward into cooler, shallower White Rim strata. Geologic evidence, including paragenetic relations between oil and early calcite cement, suggests, however, that migration did not take place until near maximum burial. The presence of "dead" oil in the White Rim on the east side of the Green River in Canyonlands National Park constrains oil migration to the period before uplift and dissection of the Colorado Plateau, which began in Oligocene to Miocene time. Therefore, the Cretaceous to middle Tertiary interval is the most favorable time for oil migration into the Tar Sand triangle.

At the time of deposition, the White Rim Sandstone was pink due to iron-stained detrital illite-smectite and early diagenetic(?) ferric oxyhydroxide grain rims. After some burial, oil migrated through the sandstones, and organic acids formed during redox reactions. Reduction of iron in grain rims caused bleaching of the sandstone. The organic acids dissolved early poikilotopic calcite cement, creating pores in which the oil accumulated. From the middle Tertiary to the present, many late diagenetic alterations have been associated with the biodegradation and water washing of oil due to the infiltration of meteoric water into the White Rim during uplift of the Colorado Plateau. These alterations include formation of widespread secondary porosity, pyrite, quartz overgrowths (second stage), ferroan dolomite, calcite, and hematite. Movement of some oil out of reservoirs occurred at this time in response to Laramide tectonism.

Stratigraphic, hydrologic, and tectonic indicators suggest that the source rock(s) was to the west of the Tar Sand triangle. Because of the estimated enormous size (30–40 billion barrels) of the original accumulation, oil must have migrated along faults and unconformities as well as through permeable beds. Possible source rocks include the Late Proterozoic Chuar Group, the Mississippian Chainman Shale and equivalents, the Middle Pennsylvanian Paradox Formation, and the Lower Permian Kaibab Limestone and Phosphoria Formation. Because of the large distance between some of these formations in eastern Nevada and western Utah and the Tar Sand triangle, a major impetus, such as west-to-east thrusting during the Sevier orogeny, may have hydrodynamically driven the oil eastward toward the Tar Sand triangle.

INTRODUCTION

The White Rim Sandstone, the uppermost formation in the Lower Permian Cutler Group in the Tar Sand triangle area in southeastern Utah, was named by Baker and Reeside (1929) for spectacular exposures between the Green and Colorado Rivers (frontispiece). It is exposed throughout most of southeastern Utah and in Canyonlands National Park where it forms prominent benches that stand out against the predominantly red Permian and Mesozoic sandstones of the Colorado Plateau. It contains the largest tar-sand[1] deposit in Utah and one of the largest tar-sand accumulations in North America. Other major tar-sand deposits in Utah are in the Uinta Basin, San Rafael Swell, and Circle Cliffs (Kerns,

[1]Tar is defined by the U.S. Department of Energy (Kerns, 1984) as "***any consolidated or unconsolidated rock (other than coal, oil shale, or gilsonite) that contains hydrocarbons (bitumen) with a gas-free viscosity greater than 10,000 centipoise, at original reservoir temperatures."

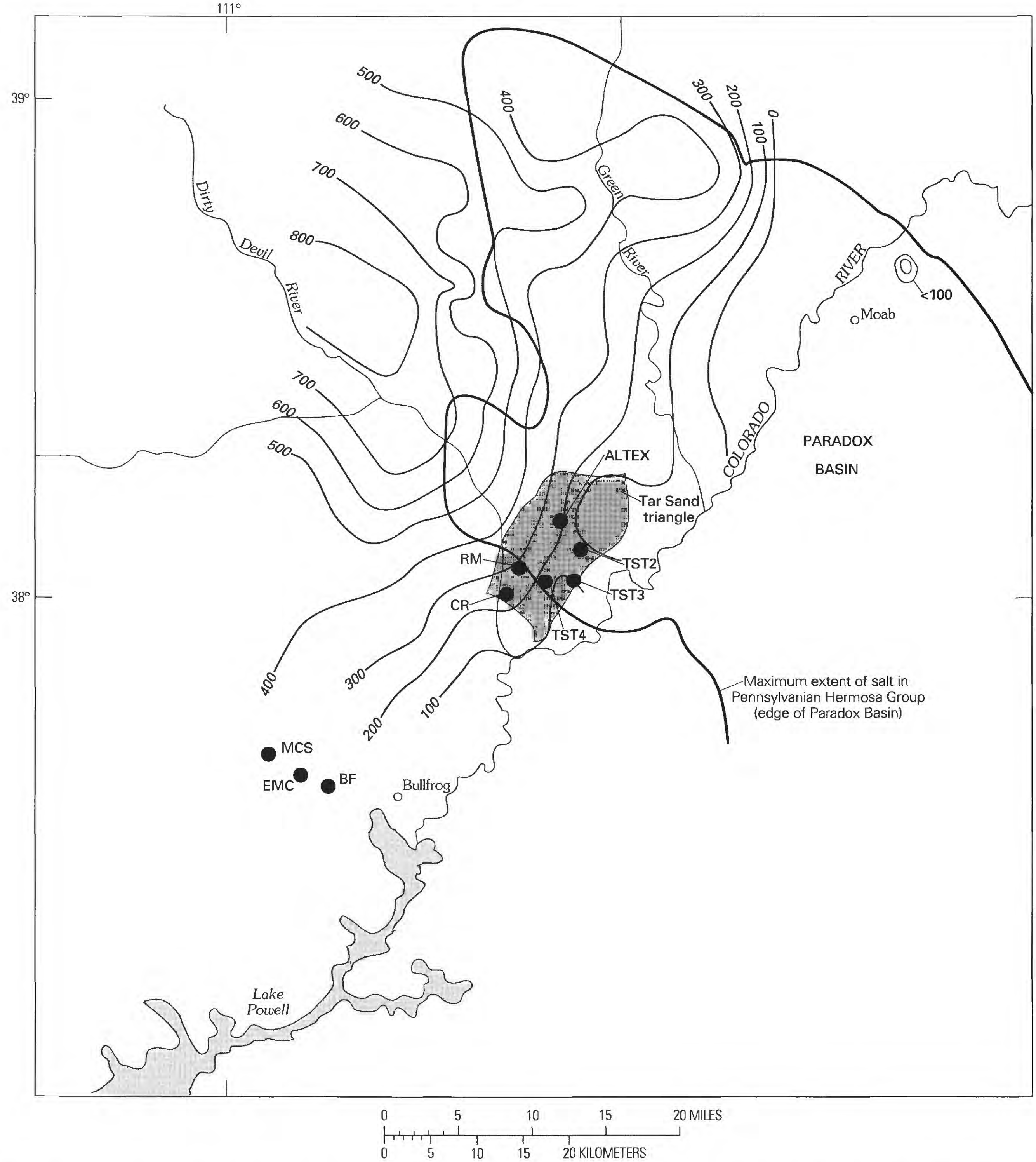

Figure 1. Isopach map of Lower Permian White Rim Sandstone, Paradox Basin, southeastern Utah, showing location of Tar Sand triangle and cores (solid circles) sampled in this study. Contour interval 100 ft (305 m); isopachs from S. Condon (written commun., 1994). Core abbreviations: RM, No. 14–15 Remington; CR, No. 33–29 Cromwell; ALTEX, ALTEX No. 1 Government; MCS, Muley Creek State No. 36–33; EMC, East Muley Creek No. 1; BF, Bullfrog No. 1.

1984, fig. 5). The Tar Sand triangle is just to the southwest of the confluence of the Green and Colorado Rivers and encompasses approximately 200 mi^2 (518 km^2) (fig. 1). It has been estimated that 30–40 billion barrels of oil were in place at one time (J. Palacas, U.S. Geological Survey, oral commun., 1994). The oil has since been biodegraded and water washed such that only about 13 billion barrels of heavy oil or tar are estimated to remain in place (Ritzma, 1979). An unknown amount of oil and volatile hydrocarbons capping the reservoir has been lost due to erosion of the White Rim Sandstone.

In the Tar Sand triangle, oil drips out of the sandstone on warm summer days (fig. 2). The oil-impregnated sandstone is as thick as 300 ft (94 m) (Campbell and Ritzma, 1979), and saturation varies from 5 to 80 percent (Dana and others, 1984). The API gravity of the oil averages 4.3, and the sulfur content (average 3.8 percent) is higher than that of other tar-sand deposits in Utah (Campbell and Ritzma, 1979). Some of the tar-sand accumulation (a few hundred acres) is not commercially available because it is in Canyonlands National Park; however, most is in the Glen Canyon National Recreation Area or on U.S. Bureau of Land Management land. Much of the land was leased by various companies in 1984 as a result of the reclassification of tar as a form of oil in 1981 (Kerns, 1984) and as a consequence of changes in regulations in the 1984 Combined Hydrocarbon Leasing Act (Dana and others, 1984). At this time, however, no tar-sand leases have been developed because the mining of tar is not economically feasible.

Although Campbell and Ritzma (1979) thought that oil was trapped in the pinchout of the White Rim Sandstone against the northwestern flank of the Monument upwarp, others have proposed that the Permian-Triassic unconformity controlled the entrapment of oil (Dolson and Henry, 1991; Huntoon, Dolson, and Henry, 1994). Dolson and Henry (1991) concluded that oil was trapped where the paleotopographic slope exceeded the structural dip (about 1°–2° NW.) and then accumulated in paleotopographic highs or dunes. The angular Permian-Triassic unconformity bevelled the top of the White Rim, but it did not impede the migration of oil because overlying conglomeratic Triassic strata are commonly oil stained. Field and petrographic observations made as part of this study reveal that oil is trapped in the more permeable sandstone of the White Rim between less permeable finer grained siltstone and sandstone of the underlying Lower Permian Organ Rock Formation and finer grained beds of the overlying Triassic Moenkopi Formation (fig. 3). In many places where the Moenkopi and Organ Rock are coarser, they are commonly oil saturated or bleached, probably as a result of the passage of hydrocarbons. The underlying Lower Permian Cedar Mesa Sandstone is also locally oil stained, as is the overlying Middle Jurassic Entrada Sandstone in the northern part of Canyonlands National Park.

According to Dolson and Henry (1991), the "feather edge" of the White Rim to the east of the Tar Sand triangle is generally devoid of hydrocarbons, but my field observations reveal "dead" oil in the White Rim Sandstone in the Island in the Sky region of Canyonlands National Park between the Green and Colorado Rivers. The local abundance of iron oxide cement and oxidized pyrite in this area suggests that a reducing environment, perhaps associated with oil-bearing fluids, was once present. Biodegradation and the slow drainage of oil southward in response to tectonics may have contributed to the present lack of oil in this area (Spencer, 1975).

Figure 2. Oil dripping out of Lower Permian White Rim Sandstone on a warm summer day in the Tar Sand triangle, southeastern Utah. Pencil shown for scale.

A source rock(s) for this huge accumulation of oil has not been identified. Because of the size of the deposit, the source rock was probably enriched by several percent in hydrogen-rich type I or II kerogen or, if organically leaner, was thick and present over a very large geographic area. In addition, for such a large accumulation to form oil migration must have been focused along very good carrier beds and (or) unconformities and faults and then very efficiently concentrated in the Tar Sand triangle area.

The primary goal of this study was to determine the time of oil migration into the Tar Sand triangle by examining the diagenetic and burial history of the Lower Permian White Rim Sandstone. Very little petrologic

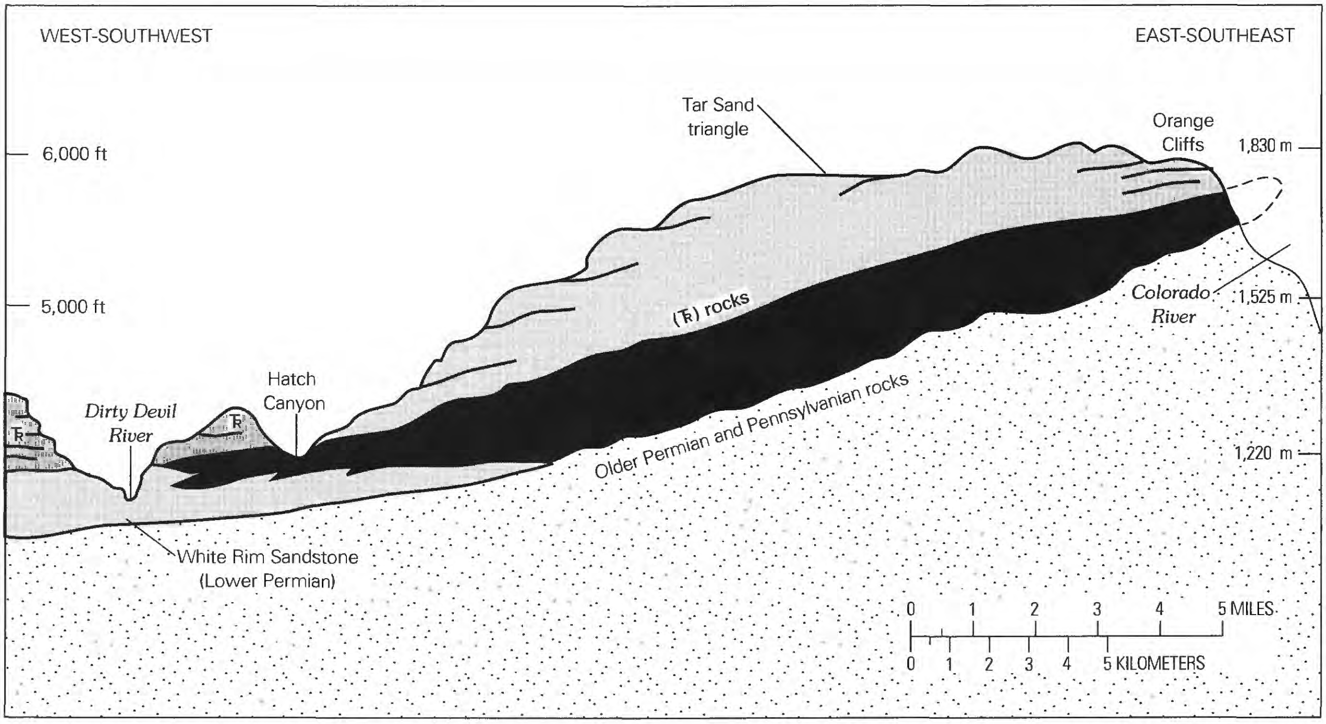

Figure 3. Schematic cross section of Lower Permian White Rim Sandstone showing extent of oil saturation (black area) in the Tar Sand triangle, southeastern Utah. Modified from Ritzma (1969).

research previously had been done on the White Rim Sandstone (Hansley, 1992, 1994; Huntoon, Hansley, and Palacas, 1994), and most of what little has been done is unpublished or based on outcrop studies such as Steele-Mallory (1981). A regional subsurface petrologic study of the diagenesis of the White Rim Sandstone has not been pubished.

Acknowledgments.—Kirkwood Oil and Gas Company, Casper, Wyo., and Marathon Technology Corporation, Denver, Colo., kindly allowed me to sample some of their cores from the Tar Sand triangle. Don McCubbin of Marathon discussed various aspects of the geology of the region and arranged for me to look at core. Jacqueline Huntoon gave me her outcrop slides to study and made helpful comments in a review of this manuscript. Several U.S. Geological Survey geologists gave me assistance: Jim Palacas was always willing to discuss potential source rocks and organic geochemistry of the Utah tar sands; Jim Schmoker provided me with data on the porosity of different dune facies; Bob Burruss allowed me to use his petrographic microscope to photograph under ultraviolet light some of my polished thin sections that contain oil-bearing fluid inclusions; Steven Condon gave me unpublished data on redefinition of the stratigraphy of the Paradox Basin, including an isopach map of the White Rim Sandstone; and Janet Pitman kindly helped me with references on carbon and oxygen isotopes. Terry Cookro critically read early versions of the manuscript. Finally, Russell Dubiel, William Keighin, and Jacqueline Huntoon greatly improved the manuscript with their thorough technical reviews.

TECTONIC SETTING

The Paradox Basin is a paleotectonic depression that formed during the Pennsylvanian Period, and it is usually defined by the maximum extent of Pennsylvanian salt (Baars and Stevenson, 1981). It is bounded on the northeast by the Uncompahgre uplift, on the southeast by the Four Corners platform and San Juan Basin, on the south by the Defiance uplift, on the southwest by the Monument upwarp, and on the northwest by the Emery high and San Rafael Swell (fig. 4). During the late Paleozoic, thousands of feet of clastic material were shed into the basin off the actively rising Uncompahgre uplift. This clastic material was composed of arkosic sediments that now comprise the Cutler Formation or Group. The basin is asymmetric; the deepest part is next to the Uncompahgre uplift, and the shallowest part is on the western side where the Tar Sand triangle is defined.

As a result of Mesozoic and early Tertiary sedimentation, the White Rim was buried under thousands of feet of sediment (11,520 ft, 3,600 m). Middle to late Tertiary uplift of the Colorado Plateau (Hunt, 1956; Lucchitta, 1972) resulted in a long period of erosion, and, as a result, the

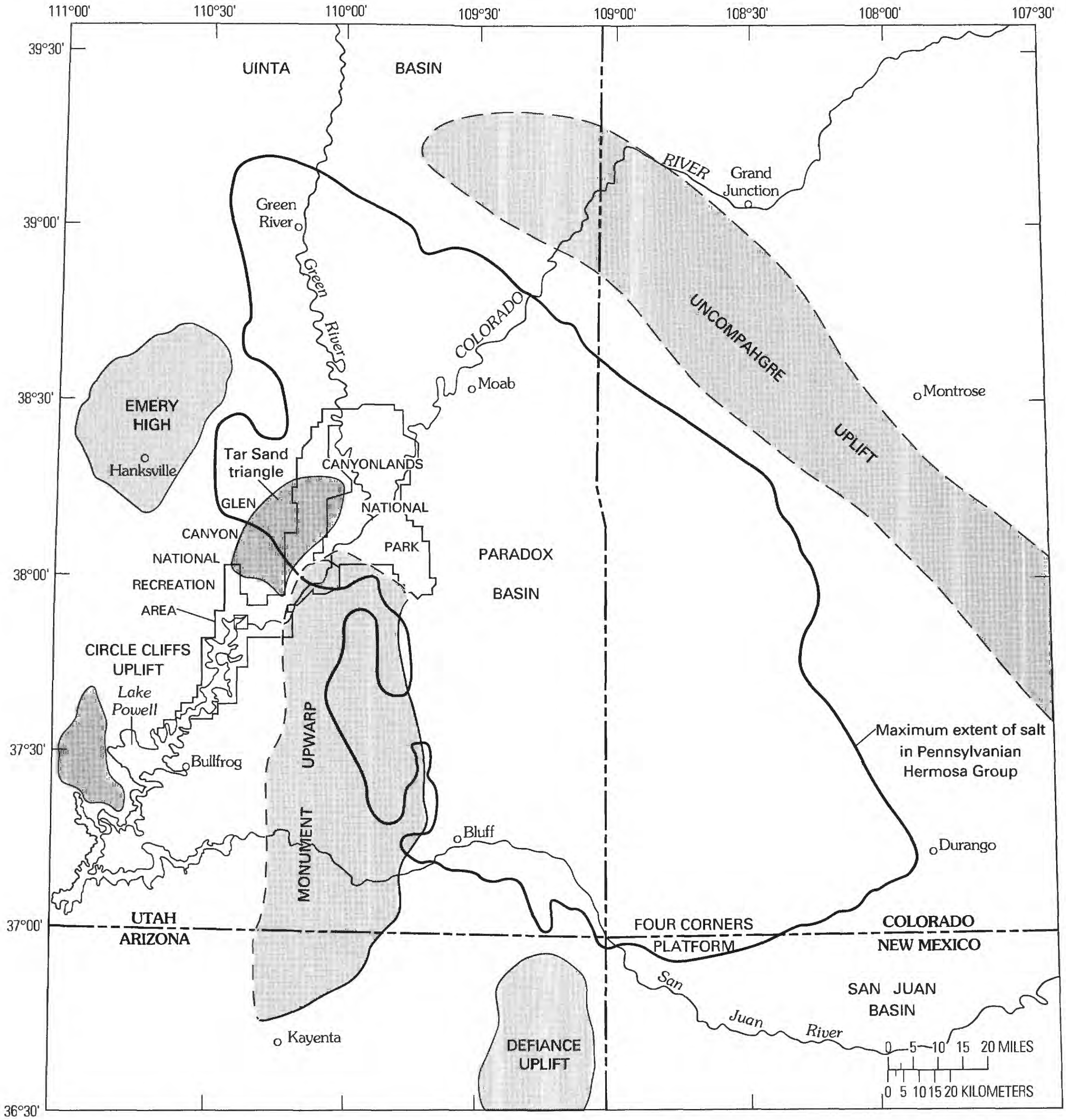

Figure 4. Tectonic features in vicinity of Paradox Basin (defined by maximum extent of salt in Pennsylvanian Hermosa Group) and adjacent areas during the Early Permian.

White Rim is now at or near the surface throughout much of the Canyonlands area.

STRATIGRAPHY

The White Rim Sandstone is considered to be the uppermost formation of the Cutler Group west of Moab, where it is well developed, and it drops to member rank in the Cutler Formation in the Moab area and to the east, where it is not as well developed (S. Condon, written commun., 1994). In the area of Canyonlands National Park and the Tar Sand triangle, it conformably overlies the Organ Rock Formation of the Cutler Group or conformable overlies the Lower Permian Cedar Mesa Sandstone of the Cutler Group. Truncation of the White Rim

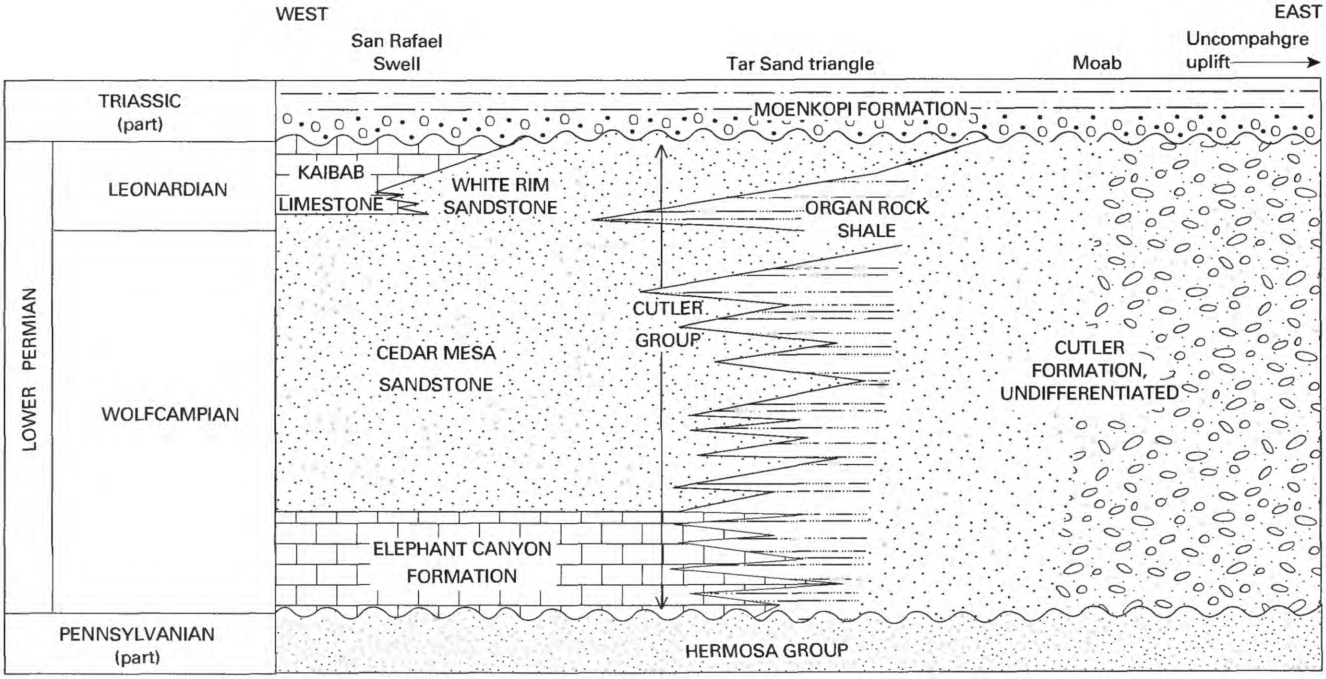

Figure 5. Relation of Lower Permian White Rim Sandstone to other Permian units in the Tar Sand triangle and vicinity, southeastern Utah. Modified from Huntoon (1985) and Huntoon, Dolson, and Henry (1994).

Sandstone by the Permian-Triassic unconformity implies that the White Rim may once have been more extensive (Huntoon, Dolson, and Henry, 1994; Huntoon, Dolson, and Stanesco, 1994; Huntoon, Dubiel, and Stanesco, 1994). According to Huntoon, Dolson, and Henry (1994), the Permian-Triassic unconformity formed between Leonardian or Guadalupian and Smithian time. In the Tar Sand triangle, the White Rim is overlain by redbeds of the Lower and Middle(?) Triassic Moenkopi Formation. To the south and west of the study area, the White Rim Sandstone is overlain by an unnamed chert-pebble conglomerate at the base of the Moenkopi Formation. This conglomerate is correlative with the lower part of the Black Dragon Member of the Moenkopi to the west in the San Rafael Swell and interfingers with the Hoskinnini Member of the Moenkopi to the east (Huntoon, Dolson, and Stanesco, 1994, fig. 2). The conglomerate locally fills channels cut into the White Rim. In Capitol Reef National Park to the west of the Tar Sand triangle, the White Rim interfingers with the Lower Permian Kaibab Limestone (Kamola and Chan, 1988; Kamola and Huntoon, 1994). The White Rim has been correlated with the De Chelley Sandstone (Lower Permian) in the Four Corners area and with the Toroweap Formation (Lower Permian) in the Grand Canyon region (Huntoon, 1985). The marine veneer appears to merge with the lower (gamma) member of the Kaibab Formation in the subsurface to the west of the Tar Sand triangle (Irwin, 1971) (fig. 5). At the tops of the No. 14–15 Remington and No. 33–29 Cromwell cores (fig. 1), the White Rim is interbedded with marine limestone that may be the Kaibab Limestone. The Kaibab is a time-transgressive unit (Kamola and Huntoon, 1994) thought to be late Leonardian to early Guadalupian in age in southern Utah (Irwin, 1971). These correlations indicate that the White Rim Sandstone is probably Leonardian in age, although Huntoon (1985) speculated that the marine veneer may be Guadalupian.

An isopach map of the White Rim Sandstone in the Paradox basin is shown in figure 1. A circular area of zero thickness just east of the Tar Sand triangle and southwest of the confluence of the Green and Colorado Rivers may reflect nondeposition of the White Rim Sandstone on the northwestern flank of the Monument upwarp (see figs. 1 and 4), which was probably intermittently rising from Pennsylvanian time through the Laramide orogeny (S. Condon, oral commun., 1994). On the other hand, it may reflect postdepositional erosion of the area, such as may have occurred during formation of the Permian-Triassic unconformity. One remnant(?) outcrop of the White Rim Sandstone, which is truncated by a fault, is in Castle Valley about 10 mi (16.1 km) northeast of Moab (fig. 1).

DEPOSITIONAL ENVIRONMENT

Some geologists have interpreted the White Rim to be primarily a shallow-marine sandstone (Baars and Seager, 1970), but it is now considered to be almost entirely eolian in origin (Baker and Reeside, 1929; McKnight, 1940; Baker, 1946; Heylmun, 1958; Steele-Mallory, 1981; Walker and Middleton, 1981; Huntoon and Chan, 1987; Steele, 1987; Chan, 1989). Sands of the White Rim were deposited in a complex erg system that included dune, interdune, sabkha, and sandsheet facies that formed in a semiarid to arid climate (Huntoon, 1985; Steele, 1987; Chan, 1989). When the White Rim erg was forming, the Kaibab ocean lay to the west and Cutler alluvial fans lay to the east (fig. 6). The White Rim erg was centered in the Dirty Devil River area and to the west and southwest of that area, where it is now present only in the subsurface. Along the edges of the erg, fluvial facies interfinger with eolian facies, and entire upright trees were engulfed in sand as the erg expanded (Chan, 1989).

The thickest part of the White Rim comprises a lower eolian unit of horizontally bedded sand-sheet facies and moderate- to high-angle crossbedded dune facies. According to Chan (1989), the dune facies constitutes 80 volume percent of the lower unit. Eolian sedimentary structures include ripples with large ripple-form indices, inversely graded laminae, grainfall strata, and avalanche tongues. Barchanoid dunes that have a unimodal orientation are in the Tar Sand triangle (Huntoon, 1985), transverse dunes are present west and southwest of the barchanoid dunes, and a sand-sheet facies is present between the Green and Colorado Rivers in the Island in the Sky region of Canyonlands National Park (Chan, 1989). Fossil fragments are generally lacking. The lower eolian unit is overlain unconformably by a thin marine unit characterized by horizontal-planar stratification, wave ripples, and fluid-escape structures (Huntoon, 1985; Chan, 1989). The marine unit may be eroded completely or as thick as 15 ft (4.3 m) (Huntoon, 1985). Megapolygons several feet in diameter are present on its upper surface (Huntoon and Chan, 1987). Because the marine unit contains reworked White Rim Sandstone grains, lithified blocks of White Rim Sandstone, and Kaibab chert pebbles, an unconformity of unknown duration is interpreted to be present between it and the underlying part of the White Rim (Huntoon, 1985).

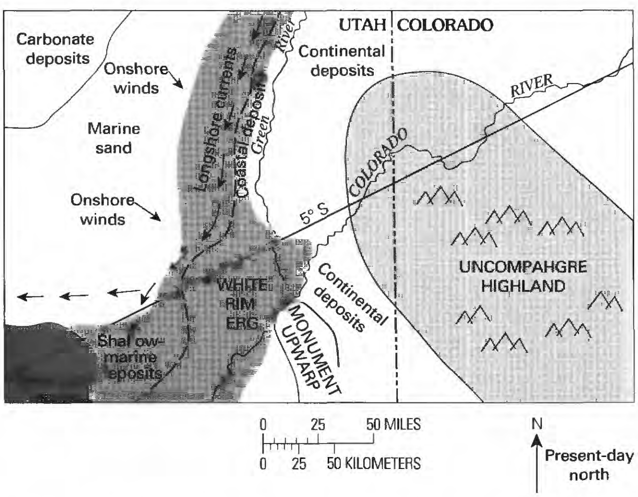

Figure 6. Paleogeography of study area during the Early Permian. Modified from Tubbs (1989).

METHODOLOGY

Although many surface samples were collected, virtually all petrographic research was done on samples from six cores collected in the Tar Sand triangle and three cores taken northwest of Bullfrog on Lake Powell in southeastern Utah (fig. 1). Outcrop samples are too altered due to recent weathering to be studied for diagenetic interpretations. Sandstones were vacuum impregnated with blue-dyed epoxy. Petrographic thin sections were stained with Alizarin Red-S (pink) for calcite, with sodium cobaltinitrite (greenish yellow) for potassium feldspar, and with potassium ferricyanide (blue) for ferroan carbonate identification. Point counts (300 points per section) of selected fine- and medium-grained sandstones determined the detrital modal mineralogy. Petrologic research was done using a petrographic microscrope with and without a fluorescence attachment, a luminoscope, an electron microprobe, and a scanning electron microscope with an attached energy-dispersive system (SEM-EDS). X-ray diffraction of the –2-µm fraction was used to identify clay minerals. Random, glycolated, and 550°C X-ray patterns were generated for each sample. Detrital heavy minerals were separated from selected samples by gravity settling in sodium polytungstate (specific gravity about 2.9).

Measurements and interpretations of fluid inclusions in authigenic dolomite in doubly polished thin sections were done by Jim Reynolds. Stable carbon and oxygen isotopes of authigenic calcite and dolomite were analyzed by Global Geochemistry Corporation (Canoga Park, Calif.), and sulfur isotopes of authigenic pyrite were determined by Krueger Enterprises (Cambridge, Mass.).

CORE DESCRIPTIONS

Locations of cores examined during this study are given in table 1. Detailed descriptions of the TST2, TST3, TST4, Bullfrog No. 1, Muley Creek State No. 36–34, and East Muley Creek No. 1 cores are given in the appendix; because of their poor condition, the No. 14–15 Remington and No. 33–29 Cromwell cores were not described. The ALTEX No. 1 Government core was described by R. Dubiel (U.S. Geological Survey, unpublished data, 1994).

Sedimentary structures are commonly obscured in oil-saturated sandstone but can be seen in unsaturated sandstone (fig. 7). Many intervals of core have a mottled or

Table 1. Location of cores and cored intervals of the Lower Permian White Rim Sandstone, southeastern Utah, examined in this study.
[Descriptions of cores given in appendix]

Core	Location	Depth below surface (feet)	
		Top	Bottom
TST2	NW¼NW¼SE¼ sec. 35, T. 30 S., R. 16 E.	1,412	>1,580
TST3	SW¼SW¼NE¼ sec. 2, T. 31 S., R. 16 E.	1,398	>1,482
TST4	SE¼NE¼NE¼ sec. 16, T. 31 S., R. 16 E.	1,395	1,525
No. 14–15 Remington	SW¼SW¼NW¼ sec. 15, T. 31 S., R. 15 E.	529	830
No. 33–29 Cromwell	SW¼SE¼NW¼ sec. 29, T. 31 S., R. 15 E.	228	487
ALTEX No. 1 Government	NW¼SW¼SW¼ sec. 26, T. 30 S., R. 16 E.	1,450(?)	1,635
Bullfrog No. 1	SE¼NW¼ sec. 21, T. 36 S., R. 10 E.	2,972	>3,042
Muley Creek State No. 36–33	NW¼SE¼ sec. 36, T. 35 S., R. 9 E.	4,028	>4,075
East Muley Creek No. 1	SE¼NE¼SE¼ sec. 19, T. 36 S., R. 11 E.	2,888	>2,954

Figure 7. Typical crossbedded Lower Permian White Rim Sandstone, East Muley Creek No. 1 core between 2,919 and 2,920 ft (889.9–890.2 m). Core diameter 4 in. (10.4 cm). Location of core shown in figure 1.

Figure 8. Typical oil-saturated Lower Permian White Rim Sandstone, TST2 core between 1,462 and 1,466 ft (445.7– 446.9 m). White beds are calcite cemented. Core diameter 4 in. (10.4 cm). Location of core shown in figure 1.

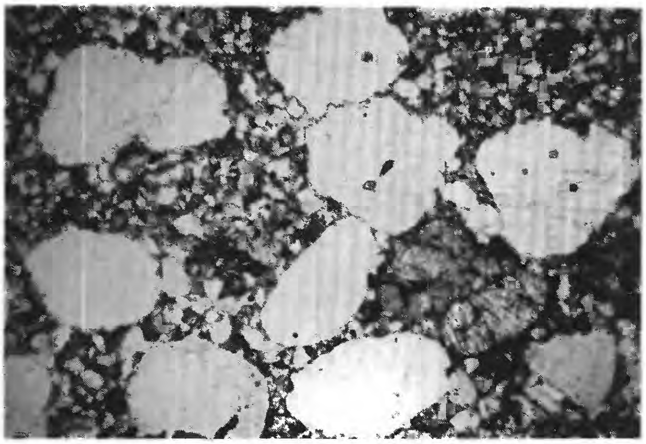

Figure 9. Photomicrograph of eolian facies of Lower Permian White Rim Sandstone, TST2 core, 1,440 ft (439 m), showing bimodal texture characteristic of eolian sandstone. Field length 3.3 mm; plane-polarized light. Location of core shown in figure 1.

banded texture resulting from the mixture of oil-saturated and calcite-cemented sandstone (fig. 8). Bedding is dominantly tabular-planar crossbedding or relatively high angle, tabular-tangential crossbedding.

The ALTEX core is oil saturated at 1,503 ft (470 m), from 1,536 to 1,585 ft (480–495 m), and at 1,628 ft (509 m). The TST2 core is oil saturated except for the interval from 1,474 to 1,480 ft (461–463 m). The TST4 core is oil saturated from 1,418 to 1,440 ft (443–450 m). The TST3 core is oil saturated intermittently at the top, at 1,412 ft (441 m), and then from 1,465 to 1,471 ft (458–460 m). The Remington core is oil saturated from the top at 480 ft (150 m) down to 672 ft (210 m) (an oil-water contact may be present between 672 and 686 ft [210–214 m]). The Muley Creek State core is only oil saturated from 4,050 to 4,061 ft (1,266–1,269 m) (an oil-water contact may be present between 4,061 and 4,063 ft [1,269–1,270 m]). The Bullfrog core has minor oil staining throughout and is the most saturated at 2,995 ft (936 m). The Cromwell core is saturated from 217 to 247.5 ft (68–77 m) and has a possible oil-water contact at 247.5 ft (77 m). The East Muley Creek core has no oil staining.

DETRITAL MINERALOGY

Detrital grains of the White Rim Sandstone are generally subangular to well rounded, and many samples display the bimodal grain-size distribution characteristic of eolian sandstone (fig. 9) (Folk, 1980). Well-rounded quartz and potassium feldspar grains are the coarsest grains in bimodal sandstones. The bimodal grain size is in horizontal laminated beds that have been interpreted as migrating interdune deposits (Kocurek, 1981). Modal analyses show that the White Rim Sandstone has a relatively simple and consistent detrital mineralogy (tables 2–10). Modal analyses of sandstones from the Tar Sand triangle cores have a 2σ of 3 with 90–96 volume percent quartz at the 95 percent confidence level (for method, see Van der Plas and Tobi, 1965); however, modal analyses of sandstones in the cores northwest of Bullfrog, which contain more potassium feldspar, have a 2σ of 4 with 81–89 volume percent quartz at the 95 percent confidence level.

Sandstones of the Tar Sand triangle are primarily quartzarenite (fig. 10), whereas those of the Bullfrog area are subarkose (fig. 11) (Folk, 1980). Outcrop sandstones from the Tar Sand triangle and Canyonlands are quartzarenite. In Folk's classification scheme, the quartz pole includes all types of quartz and metaquartzite, the feldspar pole includes all feldspars and granite and gneiss fragments, and the rock fragment pole includes fine-grained rock fragments and chert. The main feldspar in all sandstones is untwinned potassium feldspar. Chert and plutonic igneous rock fragments composed of potassium feldspar and quartz are the most common rock fragments in all sandstones. Rare flakes of muscovite are present throughout all sandstones. Thin, detrital illite-smectite (90 percent illite) grain rims are sporadically present and are most widespread in the East Muley Creek and Muley Creek State cores (fig. 12).

Nonopaque heavy minerals are well-rounded zircon, tourmaline, and apatite and rare garnet, pyroxene, amphibole, and rutile. Zircon and tourmaline each make up 30–40 volume percent of the heavy-mineral suite, and apatite makes up 18–20 volume percent. Iron-titanium oxides and magnetite are present in trace amounts.

The initial porosity of eolian sandstone varies according to the dune facies (Hunter, 1977; Schenk, 1983). For instance, tractional facies have about 38 percent porosity, grainfall facies about 43.5 percent, and avalanche-toe facies approximately 47 percent. According to Dickinson (1991), however, modern well-sorted dune sands have average porosity of only 35 percent. Because of grain overlap, Dickinson's method of estimating porosity by point-counting grains in thin sections probably underestimates the amount of porosity (J. Schmoker, oral commun., 1994).

AUTHIGENIC PHASES AND ALTERATIONS

CALCITE

In those samples totally cemented (as much as 35 volume percent) by poikilotopic nonferroan calcite, no other diagenetic minerals are present, framework grains have few contacts other than point contacts, and (apparent)

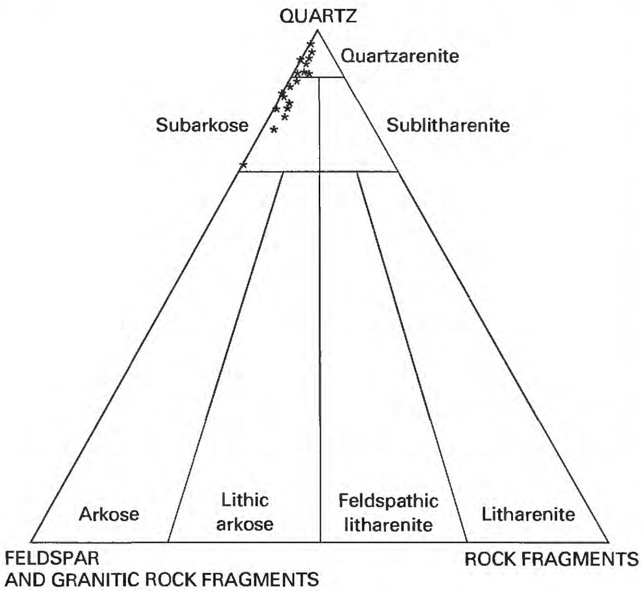

Figure 10. Lower Permian White Rim Sandstone in ALTEX No. 1 Government core, Tar Sand triangle. Sandstone classification of Folk (1980). Location of core shown in figure 1.

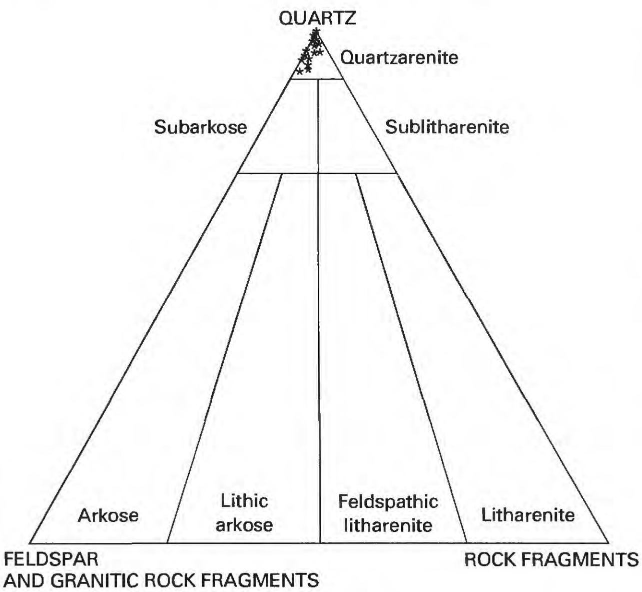

Figure 11. Lower Permian White Rim Sandstone in Bullfrog No. 1, Muley Creek State No. 36–33, and East Muley Creek No. 1 cores. Sandstone classification of Folk (1980). Location of cores shown in figure 1.

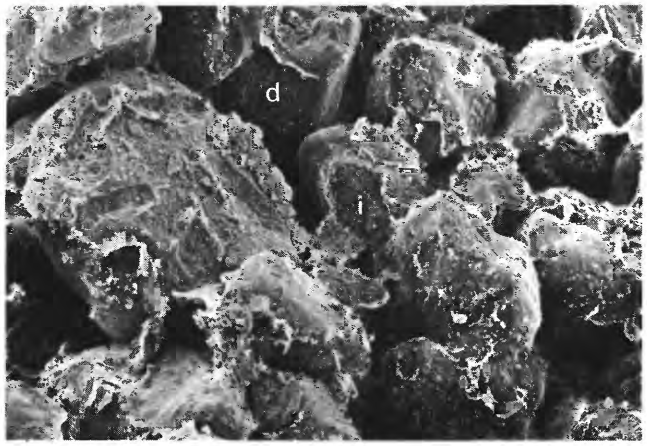

Figure 12. Scanning electron micrograph of detrital illite-smectite (i) grain rims on rounded detrital grains (d) in Lower Permian White Rim Sandstone, East Muley Creek No. 1 core, 2,954.5 ft (900.8 m). Field length 1.4 mm. Location of core shown in figure 1.

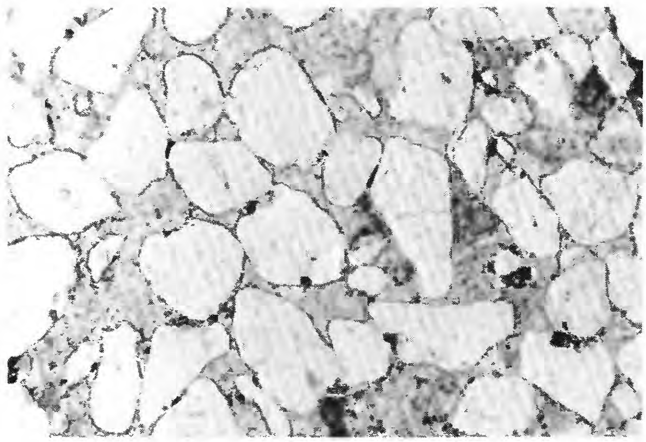

Figure 13. Photomicrograph of early poikilotopic, nonferroan calcite cement in Lower Permian White Rim Sandstone, TST2 core, 1,462 ft (445.7 m), showing floating grains and point contacts between detrital grains. Field length 3.3 mm; crossed nicols. Location of core shown in figure 1.

floating grains are relatively common (fig. 13). Near the top of the Muley Creek State core, abundant tiny (0.05 mm) calcite crystals rim framework grains and underlie quartz overgrowths. Dissolution of calcite cement has occurred over broad geographic areas, as indicated by remnants of calcite in optical continuity in all the cores. Stable carbon and oxygen isotopes of calcite cement are relatively light except for one sample (fig. 14). Ferroan calcite, or possibly ankerite as suggested by the presence of small amounts of magnesium, locally has replaced early nonferroan calcite. It is also locally intergrown with kaolinite (fig. 15).

Poikilotopic calcite cement is commonly patchy under the luminoscope (fig. 16). Electron microprobe analyses show that the patchy areas, which appear dark (nonluminescent) under the luminoscope, contain magnesium and strontium, whereas areas that appear orange and yellow under the luminoscope contain manganese. The nonluminescence is probably due to another element(s) acting as a quencher, rather than to the presence of magnesium or strontium, because neither of those elements can

Table 2. Modal analysis of TST2 core, Lower Permian White Rim Sandstone, southeastern Utah.
[Location of core shown in figure 1; numerals in sample number following hyphen represent depth below surface (in feet). 300 points counted per each thin section]

DETRITAL COMPONENTS

Sample No.	Quartz	Potassium feldspar	Plagioclase	Chert	Sedimentary rock fragments	Igneous rock fragments	Other rock fragments	Muscovite	Detrital clay	Heavy minerals
TST2-1430	209	21	4	0	0	3	4	0	3	1
TST2-1433	201	20	0	0	0	1	0	0	0	0
TST2-1448	191	19	3	0	0	0	0	0	0	0
TST2-1452	218	5	0	0	0	0	0	0	0	0
TST2-1462	227	17	2	0	0	2	2	0	0	0
TST2-1470	167	17	0	0	0	8	0	0	0	0
TST2-1474	188	22	0	2	0	3	0	0	3	0
TST2-1480	207	13	0	3	0	4	0	0	0	0
TST2-1508	201	30	1	0	1	17	0	0	2	0
TST2-1527	194	16	3	0	0	7	0	0	0	0
TST2-1535.5	185	37	3	0	0	1	0	0	2	3
TST2-1550	171	29	3	0	0	3	0	1	1	0
TST2-1553	183	18	0	0	0	3	2	0	0	0
TST2-1568	185	11	0	1	0	2	0	0	0	0
TST2-1576	208	10	0	0	0	2	0	0	0	0

AUTHIGENIC AND IMPORTED COMPONENTS AND POROSITY

Sample No.	Kaolinite	Calcite	Dolomite	Potassium feldspar	Pyrite	Petroleum	Quartz overgrowths	Void
TST2-1430	4	4	0	0	0	0	0	47
TST2-1433	0	18	0	0	0	8	7	45
TST2-1448	0	52	0	0	0	6	0	29
TST2-1452	1	35	0	0	0	12	1	28
TST2-1462	2	19	2	0	0	1	0	26
TST2-1470	0	98	1	0	0	7	0	1
TST2-1474	0	50	2	0	15	0	0	15
TST2-1480	0	22	8	0	2	0	3	39
TST2-1508	0	0	12	0	0	10	5	21
TST2-1527	0	0	2	0	1	2	25	50
TST2-1535.5	0	2	4	0	1	24	33	5
TST2-1550	1	7	14	0	0	48	20	4
TST2-1553	2	4	10	2	1	24	22	25
TST2-1568	0	69	1	0	0	5	0	25
TST2-1576	0	1	1	0	0	54	7	17

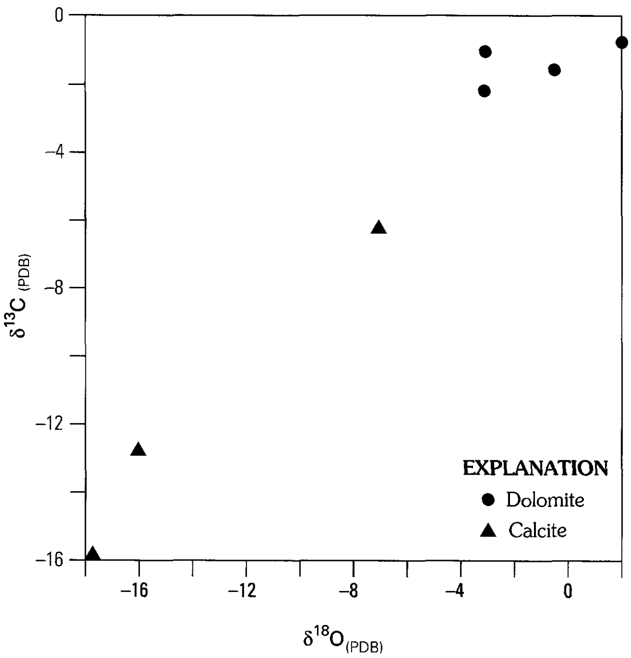

Figure 14. Stable carbon and oxygen isotopes of authigenic calcite and dolomite in Lower Permian White Rim Sandstone, TST2, TST3, and TST4 cores. Location of cores shown in figure 1.

ence luminescence because of their stable outer electron shells (D. Marshall, oral commun., 1994). The element(s) responsible for the quenching probably covaries with magnesium or strontium in the structure and is present in amounts below the limit of detectability of the electron microprobe. Surprisingly, iron content does not appear to influence luminescence as is reported for many other calcites; however, the iron content may be lower than the detection capability of the electron microprobe.

In core TST2 (1,479–1,480 ft, 450.9–451.2 m), white calcite-cemented areas with gray cores have a "chicken-wire" texture (fig. 17), similar to that of nodular anhydrite (Kinsman, 1966), suggestive of anhydrite replacement. Traces of sulfur in the calcite identified by SEM-EDS indicate that calcite probably replaced an earlier calcium sulfate cement.

QUARTZ OVERGROWTHS

Quartz overgrowths are present in all cores and are abundant in many samples, constituting as much as 11 volume percent of a sandstone in core TST2. The ALTEX core has the fewest quartz overgrowths (table 8). Quartz overgrowths usually are present in secondary

Table 3. Modal analyses of TST3 core, Lower Permian White Rim Sandstone, southeastern Utah.

[Location of core shown in figure 1; numerals in sample number following hyphen represent depth below surface (in feet). 300 points counted per each thin section]

	DETRITAL COMPONENTS							
Sample No.	Quartz	Potassium feldspar	Plagioclase	Chert	Igneous rock fragments	Other rock fragments	Muscovite	Heavy minerals
TST3-1412	193	6	0	0	0	1	1	0
TST3-1416	180	6	0	0	2	2	0	0
TST3-1418	201	14	0	0	4	4	0	1
TST3-1422	189	14	0	2	3	1	1	0
TST3-1465	223	12	2	2	3	0	0	0
TST3-1471	224	20	2	2	2	0	0	0
TST3-1473	217	16	0	1	0	0	0	0

	AUTHIGENIC AND IMPORTED COMPONENTS AND POROSITY						
Sample No.	Kaolinite	Calcite	Dolomite	Pyrite	Petroleum	Quartz overgrowths	Void
TST3-1412	0	78	2	2	10	0	5
TST3-1416	0	107	3	0	0	0	1
TST3-1418	0	74	3	0	1	0	2
TST3-1422	0	34	8	1	0	12	35
TST3-1465	2	1	7	1	10	6	31
TST3-1471	0	0	4	0	38	7	13
TST3-1473	0	14	5	0	0	1	46

Table 4. Modal analyses of TST4 core, Lower Permian White Rim Sandstone, southeastern Utah.
[Location of core shown in figure 1; numerals in sample number following hyphen represent depth below surface (in feet). 300 points counted per each thin section]

DETRITAL COMPONENTS

Sample No.	Quartz	Potassium feldspar	Plagioclase	Chert	Sedimentary rock fragments	Igneous rock fragments	Other rock fragments	Detrital clay	Heavy minerals
TST4-1402	208	18	5	8	2	4	0	0	0
TST4-1408	214	20	1	2	0	0	0	0	1
TST4-1412	222	9	0	1	0	0	0	0	0
TST4-1418	193	15	0	2	0	1	0	0	0
TST4-1421	200	32	1	2	0	1	1	4	3
TST4-1424	194	36	0	10	0	2	4	4	0
TST4-1425	191	44	3	4	0	1	1	0	0
TST4-1428	220	23	0	4	0	2	2	0	0
TST4-1440	173	21	2	5	0	1	1	0	0
TST4-1456	68	7	0	2	0	0	0	0	0

AUTHIGENIC AND IMPORTED COMPONENTS AND POROSITY

Sample No.	Kaolinite	Calcite	Dolomite	Pyrite	Petroleum	Quartz overgrowths	Void
TST4-1402	0	0	15	4	0	3	27
TST4-1408	0	2	3	0	1	5	34
TST4-1412	0	1	1	0	0	2	61
TST4-1418	0	5	5	0	53	19	5
TST4-1421	0	7	2	1	31	10	5
TST4-1424	1	19	3	2	12	0	12
TST4-1425	0	8	4	0	26	5	10
TST4-1428	0	1	9	0	0	9	25
TST4-1440	0	0	12	0	27	20	32
TST4-1456	0	3	1	1	16	2	0

Table 5. Modal analyses of Bullfrog No. 1 core, Lower Permian White Rim Sandstone, southeastern Utah.

[Location of core shown in figure 1; numerals in sample number following hyphen represent depth below surface (in feet). 300 points counted per each thin section]

DETRITAL COMPONENTS

Sample No.	Quartz	Potassium feldspar	Chert	Sedimentary rock fragments	Igneous rock fragments	Other rock fragments	Detrital clay	Heavy minerals
BF-2985	211	10	3	0	0	0	2	1
BF-2995	217	3	1	0	0	0	0	0
BF-2997	223	11	0	1	0	0	5	0
BF-3006	255	1	0	2	1	0	7	0
BF-3008	243	2	0	0	0	2	5	0
BF-3018	235	10	0	0	0	1	6	0
BF-3029	233	2	0	0	0	4	3	0
BF-3035	207	4	0	0	0	2	3	0

AUTHIGENIC AND IMPORTED COMPONENTS AND POROSITY

Sample No.	Calcite	Nonferroan dolomite	Ferroan dolomite	Pyrite	Petroleum	Quartz overgrowths	Void
BF-2985	0	52	0	2	0	4	13
BF-2995	0	12	1	6	11	2	49
BF-2997	5	1	0	0	0	22	32
BF-3006	2	5	0	1	3	5	20
BF-3008	1	3	0	0	3	8	33
BF-3018	1	19	0	1	0	0	26
BF-3029	0	8	0	0	0	31	19
BF-3035	0	27	12	3	1	20	21

Table 6. Modal analysis of Muley Creek State No. 36–33 core, Lower Permian White Rim Sandstone, southeastern Utah.
[Location of core shown in figure 1; numerals in sample number following hyphen represent depth below surface (in feet). 300 points counted per each thin section]

DETRITAL COMPONENTS

Sample No.	Quartz	Potassium feldspar	Plagioclase	Chert	Sedimentary rock fragments	Igneous rock fragments	Other rock fragments	Detrital clay	Heavy minerals
MCS-4050.5	198	2	0	0	2	0	0	0	0
MCS-4054	224	4	0	0	0	0	0	0	0
MCS-4061	223	8	0	0	0	0	0	19	0
MCS-4063.5	217	10	0	0	0	0	0	67	1
MCS-4066	214	16	1	3	0	0	0	2	0
MCS-4069	238	14	0	0	0	0	0	30	0
MCS-4075	256	6	0	2	0	1	2	8	0

AUTHIGENIC AND IMPORTED COMPONENTS AND POROSITY

Sample No.	Calcite	Pyrite	Quartz overgrowths	Petroleum	Void
MCS-4050.5	38	2	12	24	22
MCS-4054	0	1	13	9	49
MCS-4061	0	0	14	3	33
MCS-4063.5	0	2	0	0	3
MCS-4066	0	0	27	0	37
MCS-4069	0	0	2	0	16
MCS-4075	0	0	2	0	23

Table 7. Modal analysis of East Muley Creek No. 1 core, Lower Permian White Rim Sandstone, southeastern Utah.
[Location of core shown in figure 1; numerals in sample number following hyphen represent depth below surface (in feet). 300 points counted per each thin section]

DETRITAL COMPONENTS

Sample No.	Quartz	Potassium feldspar	Plagioclase	Chert	Sedimentary rock fragments	Igneous rock fragments	Metamorphic rock fragments	Other rock fragments	Detrital clay
MC-2888	260	0	0	0	0	0	0	0	2
MC-2898	240	2	0	0	0	0	1	1	0
MC-2906	251	2	2	0	0	0	0	0	23
MC-2912.5	237	3	0	0	0	0	0	1	15
MC-2916	247	4	0	5	1	0	0	0	18
MC-2937	172	10	0	3	0	0	0	1	3
MC-2952.4	219	12	0	2	0	0	0	2	4
MC-2954.5	208	2	0	1	0	1	0	0	9

AUTHIGENIC AND IMPORTED COMPONENTS AND POROSITY

Sample No.	Nonferroan dolomite	Ferroan dolomite	Pyrite	Quartz overgrowths	Void
MC-2888	4	0	0	9	25
MC-2898	0	0	1	24	31
MC-2906	1	0	0	0	21
MC-2912.5	3	2	0	0	41
MC-2916	0	0	0	0	26
MC-2937	61	15	1	0	34
MC-2952.4	25	8	0	1	27
MC-2954.5	33	10	2	0	33

Table 8. Modal analysis of ALTEX No.1 Government core, Lower Permian White Rim Sandstone, southeastern Utah.
[Location of core shown in figure 1; numerals in sample number following hyphen represent depth below surface (in feet). 300 points counted per each thin section]

DETRITAL COMPONENTS

Sample No.	Quartz	Potassium feldspar	Plagioclase	Chert	Sedimentary rock frag.	Igneous rock frag.	Metamorphic rock frag.	Other rock frag.	Muscovite	Detrital clay	Heavy minerals
TEX-1478.3	231	19	0	0	0	1	0	4	0	4	2
TEX-1479.5	192	31	0	0	0	0	0	0	3	0	0
TEX-1482.4	132	20	0	0	0	0	0	1	1	3	0
TEX-1488.2	228	8	0	0	0	0	0	0	0	1	0
TEX-1490.6	196	28	0	0	0	0	0	1	1	0	0
TEX-1503	233	10	1	0	0	0	0	1	0	0	0
TEX-1503.5	253	14	0	0	1	0	2	0	0	5	0
TEX-1510	246	10	0	0	0	2	1	0	2	21	1
TEX-1529	204	21	0	1	1	1	1	0	0	1	0
TEX-1536.5	200	5	0	0	0	2	0	0	0	0	0
TEX-1554	176	35	1	4	0	0	0	0	0	2	0
TEX-1562.1	176	30	0	0	0	0	0	0	3	5	0
TEX-1565.5	196	14	1	3	0	0	0	1	1	3	0
TEX-1569	198	12	2	2	0	1	0	1	0	0	0
TEX-1585.3	205	24	1	0	0	0	0	2	1	4	0
TEX-1587	199	28	1	0	0	0	0	4	0	0	1
TEX-1589	217	13	0	0	0	0	0	0	0	0	0
TEX-1596.5	208	34	0	2	0	0	0	3	1	8	0
TEX-1597.2	212	28	0	4	0	1	0	0	1	5	1
TEX-1616	200	18	0	1	0	0	0	0	0	0	0
TEX-1628.8	172	49	0	0	0	10	0	0	0	0	0
TEX-1633	187	23	0	0	0	4	0	1	0	0	0

AUTHIGENIC AND IMPORTED COMPONENTS AND POROSITY

Sample No.	Kaolinite	Nonferroan calcite	Ferroan calcite	Nonferroan dolomite	Ferroan dolomite	Barite	Potassium feldspar	Pyrite	Petroleum	Quartz overgrowths	Void
TEX-1478.3	14	0	24	0	0	0	0	0	0	0	3
TEX-1479.5	27	0	46	1	1	0	0	0	0	0	0
TEX-1482.4	0	18	0	34	0	0	0	110	0	0	0
TEX-1488.2	0	15	0	1	0	0	0	30	0	0	0
TEX-1490.6	0	29	0	42	0	0	0	0	0	0	0
TEX-1503	0	2	0	3	0	1	0	1	29	0	18
TEX-1503.5	2	0	0	16	1	0	0	1	0	0	2
TEX-1510	1	0	0	0	0	0	0	1	10	0	8
TEX-1529	0	0	0	6	1	0	0	0	0	0	22
TEX-1536.5	1	16	0	2	0	0	0	0	18	0	56
TEX-1554	4	0	0	3	9	0	0	27	38	0	1
TEX-1562.1	1	0	0	6	10	0	0	3	60	0	3
TEX-1565.5	0	0	0	7	0	0	0	0	50	2	8
TEX-1569	0	0	0	2	1	0	0	0	75	6	0
TEX-1585.3	3	1	0	0	1	0	10	5	14	3	24
TEX-1587	4	1	0	0	2	0	7	10	0	4	35
TEX-1589	1	2	0	0	0	0	1	0	0	6	58
TEX-1596.5	1	0	0	14	8	0	7	0	3	3	6
TEX-1597.2	0	0	0	0	6	0	15	3	0	1	12
TEX-1616	1	4	0	0	0	0	6	1	6	12	48
TEX-1628.8	6	12	1	1	1	0	3	3	30	0	12
TEX-1633	2	22	2	1	0	1	4	0	0	4	54

Table 9. Modal analysis of No. 14–15 Remington core, Lower Permian White Rim Sandstone, southeastern Utah.
[Location of core shown in figure 1; numerals in sample number following hyphen represent depth below surface (in feet). 300 points counted per each thin section]

DETRITAL COMPONENTS

Sample No.	Quartz	Potassium feldspar	Plagioclase	Chert	Sedimentary rock fragments	Igneous rock fragments	Metamorphic rock fragments	Other rock fragments	Detrital clay	Heavy minerals
RM-480	142	18	2	25	6	0	0	0	0	0
RM-493.2	120	6	0	9	0	0	0	0	0	0
RM-493.2A	167	9	0	15	0	0	0	0	0	0
RM-500	214	10	0	4	3	3	0	2	4	0
RM-506	209	5	0	5	0	0	0	0	1	0
RM-524.9	231	5	0	4	2	0	0	0	0	0
RM-558	206	35	0	4	3	10	0	4	0	0
RM-574	209	5	0	1	0	0	0	0	0	0
RM-595	219	10	0	5	1	2	0	1	0	0
RM-601	208	15	0	5	0	0	1	2	0	0
RM-622	200	11	1	7	0	0	0	0	0	0
RM-633.5	214	34	0	2	2	0	0	1	0	0
RM-652	218	14	1	1	1	0	0	4	0	0
RM-667	200	10	0	1	1	0	0	1	0	0
RM-672	204	22	0	1	0	0	0	0	0	0
RM-686	227	34	0	1	0	0	0	0	7	1
RM-745.9	226	8	1	2	0	1	0	2	1	0
RM-760.1	232	15	0	0	0	0	1	8	1	0

AUTHIGENIC AND IMPORTED COMPONENTS AND POROSITY

Sample No.	Kaolinite	Calcite	Nonferroan dolomite	Ferroan dolomite	Pyrite	Petroleum	Quartz overgrowths	Void
RM-480	0	14	7	26	0	53	6	1
RM-493.2	0	0	23	0	82	12	1	0
RM-493.2A	1	40	0	1	38	28	1	0
RM-500	3	0	0	7	0	27	6	17
RM-506	0	0	0	0	0	18	26	36
RM-524.9	3	0	0	5	0	10	10	30
RM-558	3	0	13	0	0	24	1	1
RM-574	0	0	1	4	2	21	3	54
RM-595	2	0	1	0	2	20	15	25
RM-601	1	0	4	2	1	55	3	4
RM-622	0	0	2	8	0	72	1	0
RM-633.5	3	0	0	2	0	11	0	19
RM-652	0	0	1	0	1	10	1	47
RM-667	2	0	1	1	6	18	11	47
RM-672	1	0	0	1	0	63	6	2
RM-686	9	1	4	2	0	0	6	8
RM-745.9	4	0	1	3	0	0	2	35
RM-760.1	6	0	3	0	1	0	2	34

Table 10. Modal analysis of No. 33–29 Cromwell core, Lower Permian White Rim Sandstone, southeastern Utah.

[Location of core shown in figure 1; numerals in sample number following hyphen represent depth below surface (in feet). 300 points counted per each thin section]

DETRITAL COMPONENTS

Sample No.	Quartz	Potassium feldspar	Plagioclase	Chert	Igneous rock fragments	Metamorphic rock fragments	Other rock fragments	Muscovite	Detrital clay
CR-207	173	7	0	9	0	0	0	1	0
CR-210	232	17	0	2	1	1	2	2	1
CR-233	235	13	0	0	0	0	0	0	0
CR-242.5	235	0	0	3	0	1	1	0	1
CR-247.5a	215	9	0	0	0	0	0	0	0
CR-247.5b	194	6	0	0	1	0	0	0	0
CR-268	229	28	0	1	0	0	8	0	0
CR-331	230	23	0	0	4	0	0	0	0
CR-408	229	27	0	1	3	1	1	0	1
CR-417.6	189	20	0	2	2	0	0	0	0
CR-443.5	215	22	0	1	1	0	0	0	0

AUTHIGENIC AND IMPORTED COMPONENTS AND POROSITY

Sample No.	Kaolinite	Calcite	Nonferroan dolomite	Ferroan dolomite	Pyrite	Petroleum	Quartz overgrowths	Void
CR-207	2	2	4	2	0	29	67	2
CR-210	1	7	4	0	1	0	2	30
CR-233	0	21	3	0	0	21	0	7
CR-242.5	0	0	5	0	1	4	7	19
CR-247.5a	0	54	3	0	0	13	6	0
CR-247.5b	0	0	6	0	0	28	7	58
CR-268	3	0	11	0	0	0	12	12
CR-331	7	0	6	0	3	0	13	14
CR-408	2	6	0	0	0	0	6	22
CR-417.6	7	14	1	0	0	0	29	36
CR-443.5	4	2	1	0	0	0	18	33

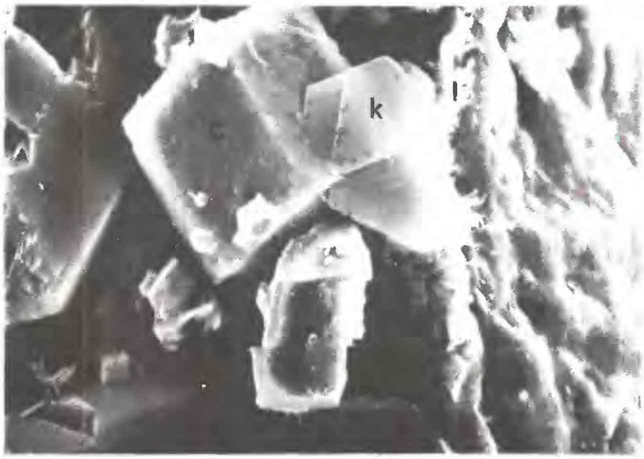

Figure 15. Scanning electron micrograph of ferroan calcite (C) containing minor amount of magnesium (ankerite?) intergrown with kaolinite (K) in Lower Permian White Rim Sandstone, ALTEX No. 1 Government core, 1,503.5 ft (458.4 m). Authigenic illite (I) is also present. Field length 30 µm. Location of core shown in figure 1.

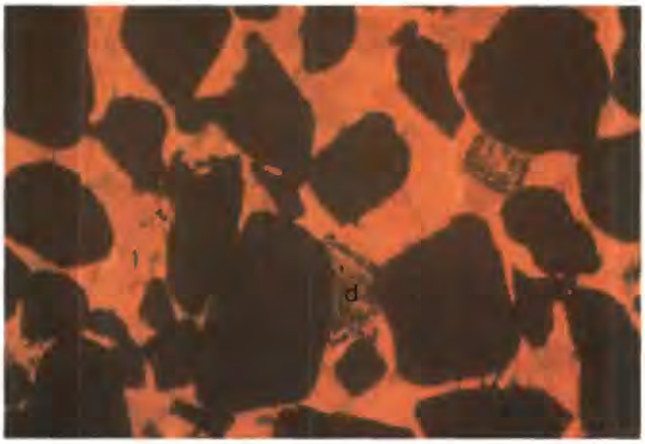

Figure 16. Cathodoluminescence micrograph showing patchy, recrystallized texture of calcite cement (yellow) in Lower Permian White Rim Sandstone, TST2 core, 1,480 ft (451.2 m). Rhombic grains are authigenic dolomite (d); dark, nonluminescent grains are detrital quartz. Field length 1 mm. Location of core shown in figure 1.

pores formed by the dissolution of early calcite cement, but locally they lie under calcite cement. In a few samples, more than one quartz overgrowth is present on a detrital grain. In his studies of Tar Sand triangle cores, P. Reimersma (Department of Energy, Laramie, Wyo., written commun., 1985) also found evidence for at least two stages of quartz overgrowths; however, the most abundant and largest overgrowths precipitated during the second stage of overgrowth formation. Oil is present under, on, and within quartz overgrowths (fig. 18).

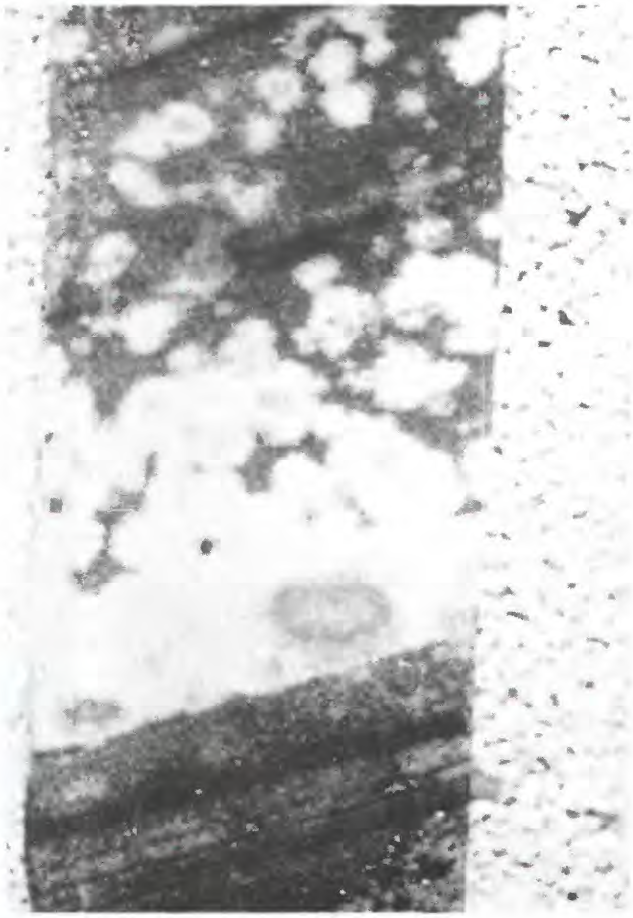

Figure 17. Photograph of "chicken-wire" texture (inherited from anhydrite?) of white calcite cement in oil-saturated Lower Permian White Rim Sandstone in TST2 core between 1,479 and 1,480 ft (450.9–451.2 m). Core diameter 4 in. (10.4 cm). Location of core shown in figure 1.

DOLOMITE

Dolomite rhombohedra of silt to fine grain size are common in all cores except for the Muley Creek State core. Most dolomite grains are cloudy as a result of included oil, and most larger rhombohedra are zoned with a nonferroan core and a small ferroan overgrowth (fig. 19). Some grains are large and clear, contain few inclusions, and enclose several detrital quartz grains. Some dolomite grains have rounded, nonferroan detrital(?) dolomite cores that luminesce red (fig. 20). Electron microprobe analyses indicate that the red color is due to co-substitution in the dolomite structure of as much as 1 weight percent iron for magnesium and traces of manganese (<1,500 ppm) for calcium. As many as ten alternating ferroan and nonferroan zones of dolomite were

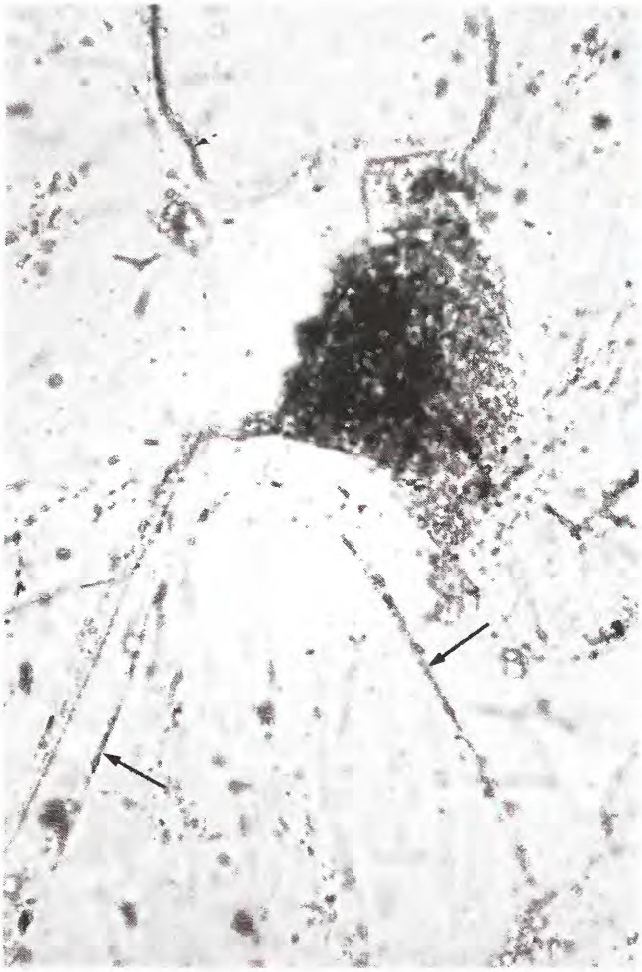

Figure 18. Photomicrograph showing oil (arrows) on and under quartz overgrowths and filling a pore in Lower Permian White Rim Sandstone, ALTEX No. 1 Government core. Field length 0.17 mm; plane-polarized light. Location of core shown in figure 1.

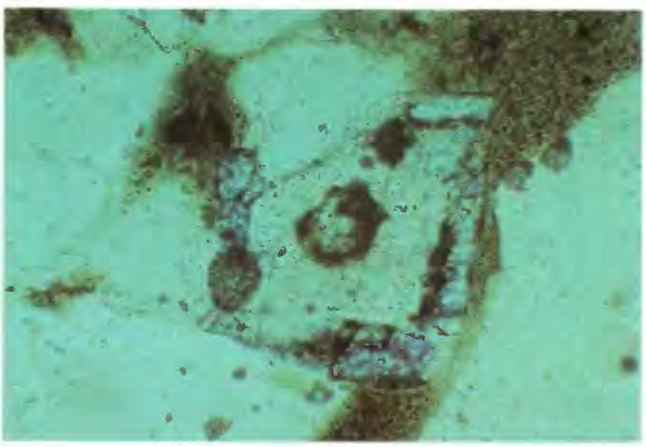

Figure 19. Photomicrograph of nonferroan dolomite grain with oil (brown) near its center and a ferroan (blue-stained) overgrowth in Lower Permian White Rim Sandstone, Bullfrog No. 1 core, 3,035 ft (925.3 m). Oil fills pores surrounding dolomite. Field length 0.4 mm. Location of core shown in figure 1.

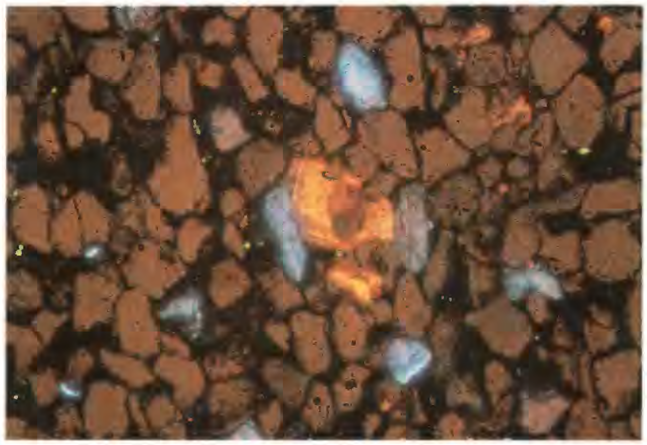

Figure 20. Cathodoluminescence micrograph of dolomite (yellow) with red (iron-bearing) core in Lower Permian White Rim Sandstone, TST2 core, 1,508 ft (459.8 m). Blue, strongly luminescent grains are detrital potassium feldspar; brown, weakly luminescent grains are detrital quartz; and black areas are voids. Field length 1 mm. Location of core shown in figure 1.

Figure 21. Photomicrograph of authigenic dolomite rhombohedron in Lower Permian White Rim Sandstone, Bullfrog No. 1 core, 3,035 ft (925.3 m), showing alternating concentric zones of ferroan (dark) and nonferroan dolomite (light). White grains are detrital quartz. Field length 0.8 mm; plane-polarized light. Location of core shown in figure 1.

observed in one crystal in the Bullfrog core (fig. 21), but most crystals have less than four zones. In multizoned crystals, the outer zone is always ferroan. SEM-EDS X-ray maps clearly show the general (qualitative) distribution of calcium, magnesium, and iron in dolomite and silicon in surrounding quartz grains (fig. 22). Many dolomite rhombohedra contain numerous two-phase hydrous inclusions (fig. 23) associated with the oil-bearing inclusions. Although most oil-bearing inclusions do not fluoresce, a few fluoresce yellow (fig. 24), indicating that not all of the oil is "dead" (degraded). Carbon and oxygen isotopes of dolomite are shown in figure 14.

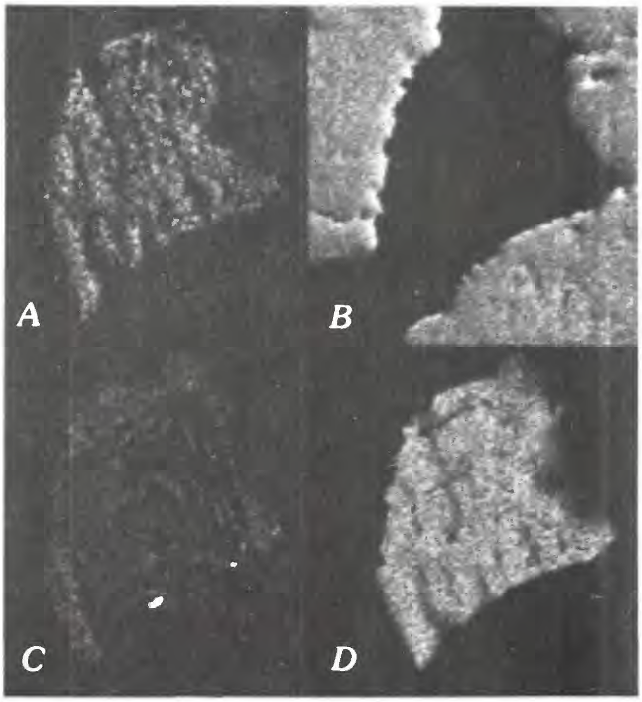

Figure 22. Scanning electron micrographs of X-ray maps generated using scanning electron microscope energy-dispersive system showing distribution of (*A*) magnesium in dolomite, (*B*) silicon in surrounding quartz grains, (*C*) iron in dolomite, and (*D*) calcium in dolomite in Lower Permian White Rim Sandstone, Bullfrog No. 1 core, 3,035 ft (925.3 m). Field length of each micrograph 0.3 mm. Location of core shown in figure 1.

PYRITE

Pyrite cement and individual pyrite crystals are closely associated with oil and are present throughout the cores in secondary pores created by the dissolution of calcite cement (fig. 25). Pyrite cement is abundant near the top of the Remington and ALTEX cores, where it appears to have partly replaced framework grains and calcite cement. Because stratigraphic control in the cores is poor, some of these samples might be at the base of the Lower Triassic Hoskininni Member of the Moenkopi Formation or unnamed Triassic chert pebble conglomerate rather than in the White Rim Sandstone. Sulfur isotopes of pyrite cement and crystals are shown in table 11.

POTASSIUM FELDSPAR

Authigenic potassium feldspar is present as rare, small overgrowths on detrital potassium feldspar grains. In the ALTEX core, small potassium feldspar overgrowths also are on detrital plagioclase grains. Individual, micron-size authigenic potassium feldspar crystals are more common than

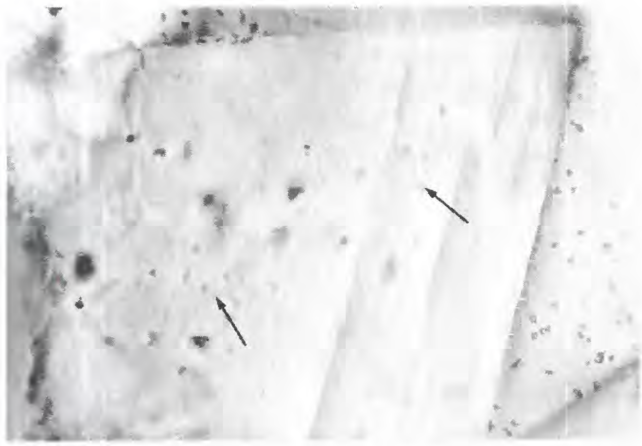

Figure 23. Photomicrograph of fluid inclusions containing vapor phases (arrows) in authigenic nonferroan dolomite in Lower Permian White Rim Sandstone, TST2 core, 1,522 ft (464 m). Field length 0.1 mm; oil immersion in plane-polarized light. Location of core shown in figure 1.

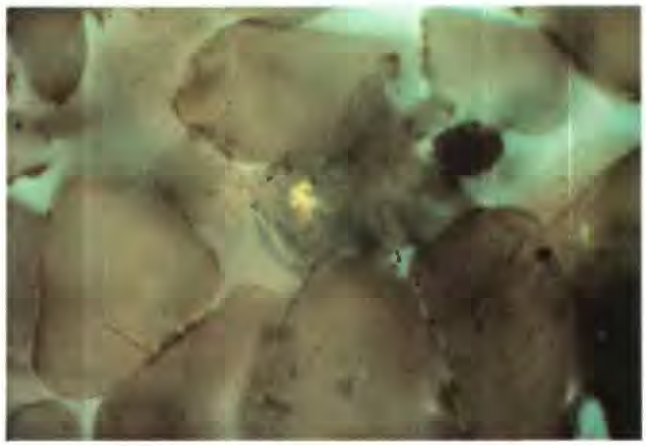

Figure 24. Photomicrograph of fluorescent (yellow) oil in authigenic dolomite in Lower Permian White Rim Sandstone, TST4 core, 1,473 ft (449.1 m). Field length 0.4 mm; short-wavelength ultraviolet light. Location of core shown in figure 1.

overgrowths, but they are only visible with the SEM. Under the SEM, they were seen on quartz overgrowths and intergrown with authigenic illite (fig. 26) and as "adularia-like" rhombic crystals only several microns in length. They are most abundant near the base of the White Rim in the ALTEX core where they are present as 20–30-µm elongate crystals that commonly contain oil in dissolution vugs (fig. 27).

CLAY MINERALS

X-ray diffractograms of the –2-µm fraction of White Rim samples showed that kaolinite is the only major authigenic clay mineral. SEM observations, however,

Table 11. Sulfur isotope ($\delta^{34}S$) values of authigenic pyrite from the Lower Permian White Rim Sandstone, southeastern Utah.

[In per mil relative to Canon Diablo troilite. Analyses by Krueger Enterprises, Inc., Cambridge, Mass. Location of cores shown in figure 1 and described in table 1]

Core	Depth (feet)	Description	$\delta^{34}S$
TST4	1,470	Pyrite crystals	–1.0
Muley Creek State No. 36–33	4,075	Pyrite crystals	–5.2
No. 14–15 Remington	493.2	Pyrite crystals and cement	–11.9
ALTEX No. 1 Government	1,482.4	Pyrite cement	+5.0
ALTEX No. 1 Government	1,488.2	Pyrite cement	+7.0

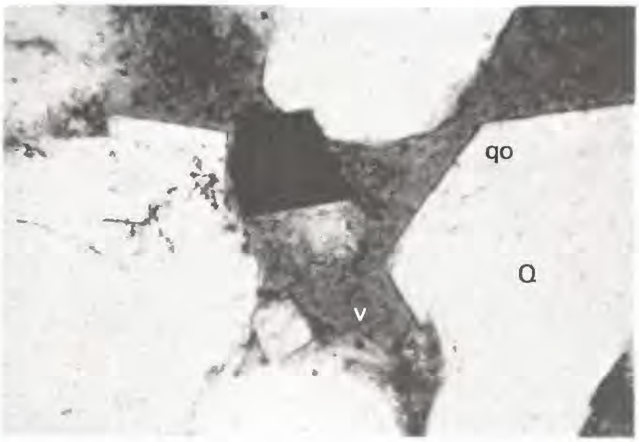

Figure 25. Photomicrograph of authigenic euhedral pyrite (black) in void in Lower Permian White Rim Sandstone, TST2 core, 1,462 ft (445.7 m). Q, detrital quartz grain; qo, quartz overgrowth; V, void. Field length 1 mm; plane-polarized light. Location of core shown in figure 1.

Figure 27. Scanning electron micrograph showing dissolution features along *c*-axis in authigenic potassium feldspar (k), Lower Permian White Rim Sandstone, ALTEX No. 1 Government core, 1,430.5 ft (436.1 m). Field length 55 µm. Location of core shown in figure 1.

Figure 26. Scanning electron micrograph of authigenic potassium feldspar (k) and illite-smectite (i) on authigenic quartz (q) in Lower Permian White Rim Sandstone, ALTEX No. 1 Government core, 1,430.5 ft (436.1 m). Field length 34 µm. Location of core shown in figure 1.

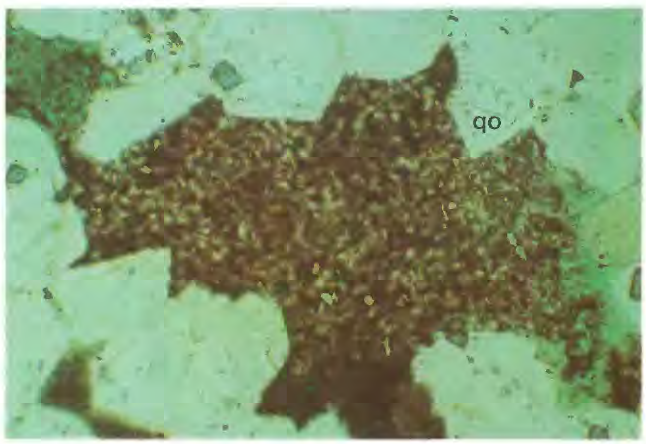

Figure 28. Photomicrograph of brown, oil-stained kaolinite in pore in Lower Permian White Rim Sandstone in No. 33–29 Cromwell core, 207 ft (63.1 m). Quartz overgrowths (qo) lie around edges of pore. Blue-dyed epoxy fills voids. Field length 0.8 mm; plane-polarized light. Location of core shown in figure 1.

revealed small amounts of authigenic illite as overgrowths on detrital illite-smectite, and authigenic kaolinite, potassium feldspar and dolomite. A low-birefringent material (chlorite?) on grains is present in some cores.

Kaolinite is present as vermicular chains of hexagonal plates in scattered pores that may have been created by the dissolution of an earlier (calcite?) cement. Because kaolinite is present in widely scattered pores, the volume percent of kaolinite as determined by modal analysis is probably lower than it actually is. Kaolinite is intergrown with ferroan calcite (fig. 15) and is commonly oil stained (fig. 28).

MINOR ALTERATIONS

Thin, amorphous iron oxide and oxyhydroxide grain coatings are present on many detrital grains. Barite is a minor cement in a few samples. Large areas of barite cement contain pyrite and oil inclusions in core TST3 (1,412 ft, 430.4 m). Anatase is an alteration product of detrital iron-titanium oxides, and hematite is an oxidation product of iron-bearing minerals such as iron-titanium oxides and magnetite.

SECONDARY POROSITY

Secondary porosity in the White Rim Sandstone is high due to leaching of early calcite cement, oil, and perhaps other, unknown phases. Remnants of calcite cement in optical continuity indicate that calcite cement was once more extensive. Because of the lack of labile framework grains, very little of the secondary porosity is intragranular or moldic. High amounts of porosity in some friable sandstones may be partly due to plucking during the thin-sectioning process.

OIL

Oil saturates much of the White Rim Sandstone in the Tar Sand triangle but is not present in sandstone that is totally cemented by poikilotopic calcite cement. Oil most commonly is present in secondary pores created by the dissolution of calcite cement. It is also present in, under, and on quartz overgrowths (fig. 18), and it stains authigenic kaolinite (fig. 28). Inclusions of oil are most common in nonferroan dolomite (fig. 20) and in fractures in quartz and potassium feldspar grains. Ferroan dolomite does not contain any oil-bearing inclusions. Dissolution cavities in authigenic potassium feldspar also contain oil. In the Muley Creek State core, oil is present in pores lined with detrital illite-smectite. The East Muley Creek core is the only core that does not contain oil.

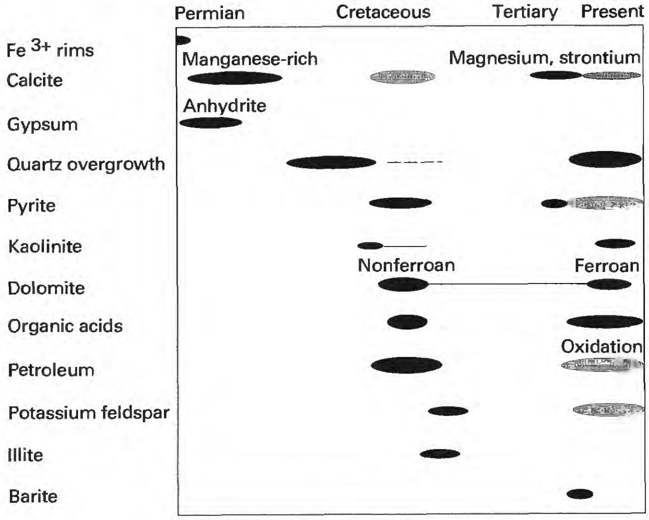

Figure 29. Paragenesis of diagenetic alterations in Lower Permian White Rim Sandstone. Shaded ellipses indicate dissolution; black ellipses indicate precipitation.

INTERPRETATION OF AUTHIGENESIS

The inferred paragenesis of diagenetic alterations in the White Rim Sandstone is shown in figure 29. In the following discussion, justifications pertaining to the placement of each authigenic mineral in the paragenetic sequence are presented.

CALCITE

The fact that samples totally cemented with nonferroan calcite have no other authigenic minerals and contain point contacts and floating grains indicates that calcite was the first cement to precipitate in the White Rim Sandstone. The high minus-cement porosity values of samples totally cemented with calcite suggest that the calcite precipitated before the sandstone was buried deeper than approximately 1,000 ft (305 m) (Conybeare, 1967, figs. 8–10). The patchy appearance of the calcite cement under the luminoscope indicates that much of it has recrystallized; however, recrystallization apparently did not affect the minus-cement porosity values, possibly because the process was slow and the cement volume did not change. An apparent inverse relation between calcite cement and oil supports the petrographic observations and conclusions (fig. 30).

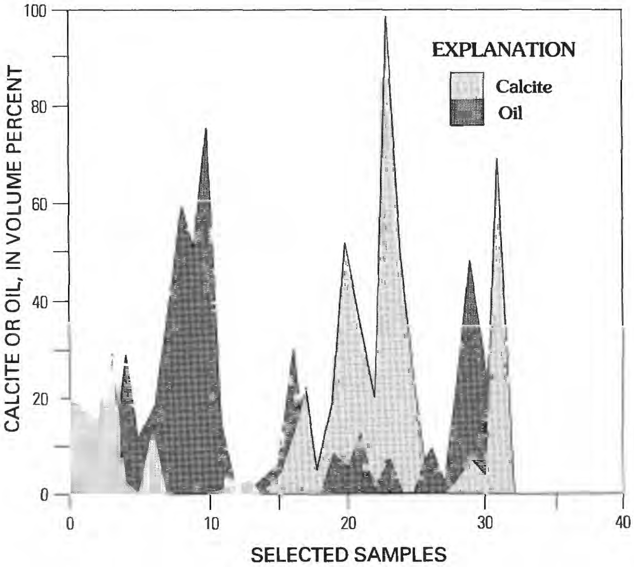

Figure 30. Relation between oil and early calcite cement in core samples of Lower Permian White Rim Sandstone.

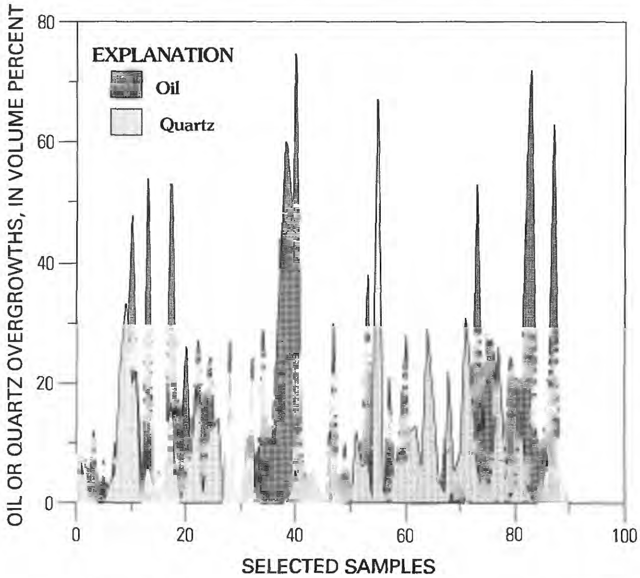

Figure 31. Relation between oil and quartz overgrowths in core samples of Lower Permian White Rim Sandstone.

The absence of calcite cement or quartz overgrowths in most of the Muley Creek State core may be due to the presence of detrital illite-smectite clay rims on virtually all detrital grains, which causes low permeability. Remnants of calcite cement and oil are present only at the top of the Muley Creek State core where there are very few detrital clay rims; perhaps permeability was high enough for groundwater to flow through the sandstone.

The small, equant calcite crystals in the Muley Creek State core were precipitated from solutions supersaturated with respect to calcite. The fact that these crystals are at grain contacts and under quartz overgrowths indicates that they formed soon after deposition.

GYPSUM

Gypsum precipitated locally where the sulfate concentration was high, perhaps close to or in an interdune environment where sabkha conditions prevailed. The gypsum later may have converted to anhydrite at 56°C; later replacement of the anhydrite by calcite preserved the "chicken-wire" texture characteristic of some anhydrite.

QUARTZ OVERGROWTHS

The lack of two-phase fluid inclusions indicates that all quartz overgrowths in the White Rim Sandstone formed at low (<50°C) temperatures (Goldstein and Reynolds, 1994). Because few detrital quartz grains show any dissolution and because a large volume of quartz overgrowths is present in some samples, a large volume of silica was apparently imported into the sandstone. A major problem is the low solubility of silica in most solutions: seawater, 6.2 mg/kg, and river water, 10.4 mg/kg (Meybeck, 1979). Some quartz overgrowths may have formed from silica imported in the form of silica–organic acid complexes during the migration of oil. Organic compounds are good complexing agents for silicon because they increase the solubility of silica near pH 7 (Bennett and Siegel, 1987, 1991). Many quartz overgrowths may have formed during late diagenesis when meteoric water recharge percolated through the White Rim Sandstone as a result of uplift of the Colorado Plateau. Because of the low concentrations of silica in meteoric water, large volumes of freshwater would have been necessary to transport by inorganic means the quantity of silica required to form the volume of late quartz overgrowths that are present in the White Rim. In a study of the Lower Cretaceous Parsons Group sandstones in Canada, Potocki (1989) concluded that freshwater recharge accounted for the transport of large volumes of silica. In the absence of interlayered shale or clay-mineral transformations (smectite to illite), either of which might provide silica or dissolved organics to complex with silica in the White Rim, freshwater recharge is the most likely mechanism for obtaining large amounts of silica.

Late overgrowths were able to grow larger into oversize secondary pores, and they may have incorporated oil at that time. The precipitation of quartz overgrowths in response to processes related to the biodegradation of oil created an inverse relation between quartz overgrowths and oil (fig. 31).

DOLOMITE

Some nonferroan dolomite is interpreted to have precipitated at the same time that oil migrated into the White Rim sandstones because of the presence of oil inclusions along growth zones within dolomite rhombohedra. Other dolomite rhombohedra are surrounded by oil and apparently precipitated before the introduction of oil. Some rhombohedra may have formed around a drop of oil already present. The round, red-luminescent cores of many dolomite rhombohedra may have been derived from adjacent interdune deposits. Dolomite overgrowths commonly grew on these detrital dolomite nuclei. The outermost part of the overgrowths is always ferroan, suggesting precipitation from fresher water, which generally contains more iron than seawater, during uplift of the Colorado Plateau. The lack of vapor-phase inclusions in ferroan dolomite indicates that the ferroan dolomite formed at temperatures below 50°C.

Compositionally zoned carbonate crystals are common in sedimentary rocks. According to Machel and Burton (1991), at least 26 factors may contribute to differences in composition, and thus differences in luminescence, of crystals. These factors include temperature, salinity, concentrations of activators and quenchers, Eh, kinetics, microbial activity, diagenesis, fluid flow, and crystal surface structure. One favored explanation for zoning is that changes in precipitation rate can lead to differences in partitioning of trace elements into dolomite and calcite (Reeder and Prosky, 1986; Paquette and Reeder, 1990). Variations in both temperature and distribution coefficients (dependent on crystal growth rate) of iron and perhaps other trace elements or activators-quenchers in the dolomite have been suggested as a cause of zoning by Dromgoole and Walter (1989); however, Wogelius and others (1992) showed that the precipitation rate would have to change by about four orders of magnitude to produce a ferroan dolomite. This change would necessitate a very large change (more than five times) in the equilibrium ion activity product that would have to be caused by a very large variation in composition of the fluid.

The most commonly suggested cause for concentric zoning such as that in the White Rim dolomites is a change in the Eh of the groundwater because the elements that are usually involved in the zoning (manganese and iron) are Eh sensitive as a result of their occurrence in more than one valence state. Fraser and others (1989) observed that the pronounced concentric zoning in dolomite from limestone in Italy resulted from variations in the concentrations of iron, manganese, and zinc, all redox-controlled elements. Variations in Eh controlled the distribution of manganese and iron between the pore fluid and manganese- and iron-oxyhydroxides and thus influenced the activities of these elements in solution. Zinc is not directly controlled by changes in Eh; however, its solubility is governed by the effects of Eh-pH on sulfide-sulfate equilibria and by the release of zinc into solution after reduction of manganese- or iron-oxyhydroxides.

The most likely mechanism for formation of the zoned carbonate crystals in the White Rim, especially those that contain many concentric zones, is a fluctuating interface (oil-water contact?) between a reducing oil-bearing water and a less reducing, non-oil-bearing brine(?). This explanation is plausible because of the oscillatory nature (ferroan-nonferroan) of the zones and the fact that the dolomite crystals having the most zones are present in small vertical intervals in the cores, particularly in the Bullfrog core. The fact that the outermost zone is always ferroan and is interpreted to have precipitated during late diagenesis may reflect formation during uplift of the Colorado Plateau and percolation of meteoric water through the White Rim Sandstone.

PYRITE

Most pyrite cement in White Rim sandstones apparently precipitated at the same time as the oil or perhaps earlier because the cement completely surrounds framework grains in some samples. Another generation of pyrite crystals that are associated with ferroan dolomite precipitated in secondary pores, possibly during biodegradation of oil. During oxidation of the oil, some pyrite was locally oxidized to barite and hematite.

POTASSIUM FELDSPAR

Small amounts of authigenic potassium feldspar may have been furnished by dissolution of detrital potassium feldspar within the White Rim Sandstone; however, the large amounts of authigenic potassium feldspar in the ALTEX core strongly suggest that some potassium was imported into the sandstone. Perhaps a potassium-rich brine migrated upward along faults from the underlying Middle and Upper Pennsylvanian Hermosa Group, which contains potash deposits (Phillips, 1975). Dissolution of sylvite and carnallite in the Hermosa is thought to have occurred during the Tertiary (S. Williams-Stroud, U.S. Geological Survey, oral commun., 1994). Abundant authigenic potassium feldspar overgrowths and micrometer-size crystals associated with dolomite near the bottom of the ALTEX core suggest precipitation from a brine or in a mixing zone between a brine and freshwater.

CLAY MINERALS

Kaolinite precipitates from freshwater (Bjorlykke, 1979); therefore, meteoric water invaded the White Rim Sandstone at some time during its postdepositional history. Textural relations suggest that kaolinite precipitated before the migration of oil because kaolinite is locally saturated with oil. Kaolinite may have formed, however, during biodegradation of the oil when conditions were acidic. Periods of meteoric recharge before oil migration, during which the kaolinite may have precipitated, include the Triassic, when the climate is interpreted to have been monsoonal (Dubiel and others, 1991), the Jurassic, when rejuvenation of the Uncompahgre uplift occurred (Sanford, in press), and the middle to late Tertiary, when the Colorado Plateau was uplifted. Intergrowth of kaolinite and ferroan calcite indicates that they were cogenetic.

Illite overgrowths on kaolinite indicate that illite formed after kaolinite. Intergrowths of illite and authigenic potassium feldspar indicate that these two authigenic minerals are cogenetic.

SECONDARY POROSITY

Most porosity in White Rim sandstones is interpreted to be secondary and to have formed during two major episodes of dissolution. The first episode occurred when organic acids related to the influx of oil dissolved early calcite cement. Organic acids can dissolve carbonates and silicates and are known to be present in significant concentrations in oil-field brines (Kharaka and others, 1986). The second episode occurred during the biodegradation of oil when the White Rim was infiltrated by meteoric water. At this time the formation water became acidic due to biodegradation of the oil that resulted in the release of organic acids and carbon dioxide. Secondary porosity that formed during biodegradation allowed for movement of oil into different areas of the sandstone.

STABLE ISOTOPES

CALCITE

All calcite samples chosen for isotopic analyses contained what, under the petrographic microscope, appeared to be early nonferroan calcite cement. Shortly after the time of deposition, porewaters in the White Rim Sandstone were probably marine because of the transgression of the Kaibab sea (Kamola and Huntoon, 1994). The relatively light $\delta^{13}C$ values for three of the calcite samples suggest that the carbon is a mixture of inorganic (heavier) and organic (lighter) carbon (Longstaffe, 1987). The $\delta^{13}C$ value for early calcite cement that precipitated from marine water should be near zero per mil, whereas calcite that incorporated only organic carbon should be much lighter (–30 per mil; Hoefs, 1987). Because the White Rim is an eolian sandstone, there was little or no organic matter within it at the time of deposition to contribute isotopically light carbon. Therefore, the light values of the early calcite suggest that early formed calcite reequilibrated during later diagenesis when light carbon was available due to biodegradation of the oil.

Oxygen isotope values values for the three samples that have light carbon isotopes are lighter than would be expected for early calcite cements that precipitate from marine water (Longstaffe, 1983, 1987); however, these isotopes probably also reequilibrated during recrystallization because carbonates exchange oxygen with water more readily than do silicates (Clayton, 1959; Keith and Weber, 1964). The patchy luminescence of the calcite indicates that this was indeed the case. Oxygen isotope values for these calcites are light, probably as a result of exchange with ^{18}O-poor meteoric waters during late diagenesis. Oxygen isotopes are sensitive to changes in both temperature and salinity: $\delta^{18}O$ values decrease as temperature increases and increase as salinity increases (Hoefs, 1987). Because the recrystallization event is interpreted to have taken place during and (or) after uplift of the Colorado Plateau, it is more likely that the depleted oxygen isotope values are a result of decreased salinity due to the influx of meteoric water.

The sample of calcite cement that has the heaviest carbon and oxygen isotope values apparently was not affected as much by recrystallization because its values of –6.23 per mil for $\delta^{13}C$ and –6.9 per mil for $\delta^{18}O$ more closely approximate those of seawater, which was probably the formation water soon after burial.

Averaging the $\delta^{18}O_{SMOW}$ values for the three lightest calcites, the $\delta^{18}O_{SMOW}$ value for water from which the calcite would have precipitated is –15.5 per mil (for method, see Friedman and O'Neil, 1977). This relatively light value probably includes a significant component of meteoric water, which also suggests that the early calcite cement reequilibrated during diagenesis. The $\delta^{18}O_{SMOW}$ value for the water from which the other calcite cement precipitated is –5.1 per mil at 15°C, reflecting somewhat less meteoric input.

DOLOMITE

Samples of dolomite that contain the least zoning were chosen for isotopic analysis, but their isotopic values probably still represent a mixture of at least two stages of dolomite precipitated from two different waters. Because the nonferroan part of a dolomite rhombohedra is usually much larger, the isotope values primarily represent that composition. Neither the oxygen nor the carbon isotope values deviate appreciably from values for marine limestone; thus, the dolomite most likely precipitated from waters close to seawater in composition or from a mixture of a brine and freshwater. The lighter carbon isotope values reflect a small input from organic carbon. Isotopic formulas calculated for dolomite by Friedman and O'Neil (1977) show that the water, which would have been in equilibrium with the nonferroan dolomite containing oil-bearing and two-phase inclusions with homogenization temperatures clustering around 85°C, would have had a $\delta^{18}O_{SMOW}$ of +7.81 per mil. This heavy value suggests that the dolomite precipitated from an evolved formation water more saline than seawater.

PYRITE

The heaviest $\delta^{34}S$ values are the +5 and +7 per mil values for pyrite cement at the top of the ALTEX core. At least four explanations are possible for the genesis of the heavy pyrite cement. (1) Organic sulfur derived from oil reacted with ferric iron in the grain-rimming clay or oxyhydroxides releasing sulfur in the form of hydrogen sulfide gas, which then reacted with ferrous iron to form pyrite (organic sulfur $\delta^{34}S$ values vary from −10 to +35 per mil; Tissot and Welte, 1984). A range of pyrite $\delta^{34}S$ values would result from this process. (2) Bacterially mediated sulfate reduction in a closed system resulted in heavier and heavier sulfur isotope values (Hoefs, 1987). (3) Diffusion of hydrogen sulfide gas upward from the underlying petroleum reservoir during (late) biodegradation of the oil and entrapment of this gas below the impermeable Moenkopi beds is responsible for the abundance of pyrite cement at the top of the permeable White Rim. (4) Because the $\delta^{34}S$ value of the Permian ocean was about +10 per mil (the heaviest in geologic history; Hoefs, 1987), the pore waters initially contained heavy sulfur. Because the pyrite cement most likely precipitated during early diagenesis, the last explanation is favored with possibly some contribution from bacterially mediated sulfate reduction (explanation 2).

The slightly lighter $\delta^{34}S$ values of the individual, late pyrite crystals probably reflect a mixture of sulfur derived from different processes. Many of these crystals are in secondary porosity apparently associated with the biodegradation of oil after uplift of the Colorado Plateau when formation temperatures were cool enough for bacterial reduction of sulfate to take place.

BLEACHED SANDSTONE

Bleaching of the White Rim Sandstone may have been caused by the passage of oil and associated organic acids. The White Rim is whitish gray in outcrop everywhere that it is not oil saturated and in the subsurface with the exception of the East Muley Creek core. Although the White Rim may have been white at the time of deposition, the fact that the East Muley Creek core is not bleached (and does not contain oil) suggests that most bleaching is diagenetic. Round, bleached spots in many red beds contain traces of organic matter, suggesting that the bleaching was the result of reduction processes caused by presence of organic matter (Hofmann, 1992). Surdam and others (1993) proposed that ferric iron in clay or iron oxyhydroxide coatings on sand grains are reduced to ferrous iron by oil-bearing solutions. This mechanism for the bleaching of red beds may be applicable to the White Rim. Organic acids that are produced by the (redox) reaction of oil with ferric grain coatings dissolve calcite cement and thus create secondary porosity. Ferrous iron is then carried by organic complexes to sites of precipitation where it combines with sulfur and is incorporated into pyrite. The sulfur is provided by organic matter or by reduction of sulfate. The East Muley Creek core apparently remained pink due to pervasive, thicker grain rims that decreased its permeability, thus preventing the influx of oil-bearing solutions.

FLUID INCLUSIONS

Although it is not certain that they are primary, the micron-size, two-phase hydrous inclusions in oil-bearing, authigenic nonferroan dolomite meet two important recognition criteria for primary inclusions: (1) consistent liquid to vapor phase ratios of inclusions within one crystal and (2) occurrence in crystal growth zones (Goldstein and Reynolds, 1994; J. Reynolds, written commun., 1994). Homogenization temperatures (n=30) of the inclusions are between 65°C and 100°C, and most are tightly clustered (n=23) between 80°C and 90°C. These temperatures represent, at the very least, minimum temperatures of formation for the dolomite. Many inclusions are single phase, either all-liquid or solid, but more research is needed to determine the phase present. All-liquid inclusions could have resulted from necking, metastability, or entrapment below 50°C (Goldstein and Reynolds, 1994).

PROVENANCE

Johansen (1988) proposed that the source area for all upper Paleozoic eolian sandstones in the southwestern United States was somewhere to the northeast on the North American craton. Because of the orientation of the continent and the position of the Equator during the Permian, trade winds would have blown sand to the southwest from areas that are now in Alberta and Wyoming where thick sections of Pennsylvanian strata were eroded prior to the Permian (Johansen, 1988). Sea-level fall during late Paleozoic Gondwana glaciations may have facilitated this process by periodically exposing shelf sediments to erosion. Unfortunately, this hypothesis cannot be tested because the source rocks formerly exposed in this area have been eroded.

The Uncompahgre uplift would appear to be the most likely source area for the White Rim Sandstone because of its proximity (fig. 4) and the abundance of quartz and potassium feldspar in both Uncompahgre uplift and the White Rim; however, prevailing northwest winds (Poole, 1962; Huntoon, 1985) during White Rim deposition rule out an easterly source. Huntoon (1985) suggested that detritus may have been shed from the northern part of the Uncompahgre highlands or from the Middle and Upper Pennsylvanian and Lower Permian Weber Sandstone in the Emery high, moved southward by longshore currents, and then carried southeastward by northwesterly winds. On the basis of crossbedding directions, Baars (1962) suggested that the White Rim is composed of reworked Cedar Mesa Sandstone for which source rocks were somewhere to the northwest; however, the White Rim Sandstone is more quartzose (subarkose) than the underlying Cedar Mesa Sandstone or Cutler Formation and (or) Group (arkose) (Mack, 1978). This difference in mineralogy could be explained by mechanical winnowing, diagenesis, and (or) a different source area. Scott (1965) suggested, on the basis of the abundance of brown tourmaline and a low zircon to zircon+tourmaline ratio, that the Cedar Mesa, De Chelley, and White Rim Sandstones all had the same source. The Cutler Formation and (or) Group is almost devoid of brown tourmaline and has a high zircon to zircon+tourmaline ratio.

The freshness and abundance of detrital potassium feldspar grains in the White Rim Sandstone indicate that they were not reworked and did not travel far from the source area. Thus, a source area to the northwest is most likely, perhaps the Emery uplift and (or) the northern part of the Uncompahgre uplift or an unknown area from which the source rocks have been eroded. Chert in the White Rim would have had to come from sedimentary rocks in the source area because the Uncompaghre uplift is composed of plutonic igneous and metamorphic rocks (Werner, 1974). Chert pebbles in the marine veneer could have been reworked from the Kaibab Limestone, which contains chert to the west in Capitol Reef National Park (Kamola and Huntoon, 1994).

The greater abundance (as much as 16 volume percent) of detrital potassium feldspar in the Tar Sand triangle cores as compared to that (as much as 5 volume percent) in the three cores to the south may indicate that the source area was to the north and that fewer feldspar grains were transported to the south because of the longer distance. Diagenesis apparently did not play a role in the different amounts of feldspar because the Tar Sand triangle cores, which contain the most potassium feldspar, also contain the most diagenetic alteration. The Bullfrog area cores contain significantly less diagenetic alteration.

The lack of detrital plagioclase in the White Rim and correlative sandstones may be explained by selective weathering in the source area or by mechanical abrasion and chemical weathering in transport. The lack of textural evidence, such as moldic porosity or partly dissolved plagioclase grains, does not support diagenetic removal of detrital plagioclase from the White Rim Sandstone.

BURIAL HISTORY OF THE TAR SAND TRIANGLE

Burial history reconstructions of the White Rim Sandstone in the Tar Sand triangle were generated (fig. 32) by using thicknesses of units in stratigraphic columns (Hintze, 1988) near the Tar Sand triangle and by estimating thicknesses of eroded sediments represented by major unconformities (J. Huntoon, written commun., 1994). A constant heat flow of 50 mW/m^2 was chosen for the area (Bodell and Chapman, 1982). A mean annual surface temperature of 15°C was used because of the proximity of southeastern Utah to the Equator during the Permian. Uplift of the Colorado Plateau began about 24 Ma, in the late Oligocene to early Miocene (Lucchitta, 1972). A major unknown factor is the amount of sediment that was deposited during Cretaceous and early Tertiary time and then stripped by erosion from middle Tertiary time to the present. Extrapolation from Cretaceous and Tertiary sections in the Uinta Basin (Hintze, 1988) and in the Book Cliffs–Piceance Basin area to the northeast of the Tar Sands triangle, where there is about 10,000 ft (3,049 m) of strata (Dyman and others, 1994, fig. 7), indicates that approximately 5,750 ft (1,753 m) of Cretaceous and early Tertiary sediments was probably deposited over the White Rim Sandstone in the Tar Sand triangle area. This value may be too high because the Tar Sand triangle is on the northwestern slope of the Monument upwarp, which probably began to rise in the late Paleozoic (Huntoon, Dolson, and Henry, 1994) and rose intermittently through Laramide time. The burial and temperature reconstructions (fig. 32) for the White Rim Sandstone show that it was most deeply buried at approximately 11,520 ft (3,600 m) in late Oligocene to early Miocene time (24 Ma) when formation temperatures would have been about 90°C.

POTENTIAL SOURCE ROCKS

Many of the lighter hydrocarbons in the White Rim Sandstone are gone because of the biodegradation of the oil, but heavy biomarkers, such as triterpanes and steranes, are usually present. Nevertheless, the source rock(s) for this large accumulation of oil has not been identified. Organic geochemical comparisons of tar seeps and oils in the region show that tar seeps in the Tar Sand triangle, San Rafael Swell, and Circle Cliffs area may have been derived from carbonate source rocks (Dembicki and others, 1986). Gas chromatography and mass spectrometry spectra of oil from the Muley Creek State core also suggest that the source rock was a carbonate or phosphorite (J. Palacas, oral commun., 1993). Oil did not migrate from east to west due to paleohydrologic gradients (Sanford, in press) but travelled from some component of west to east or vertically through faults into the White Rim Sandstone. Most groundwater flow has

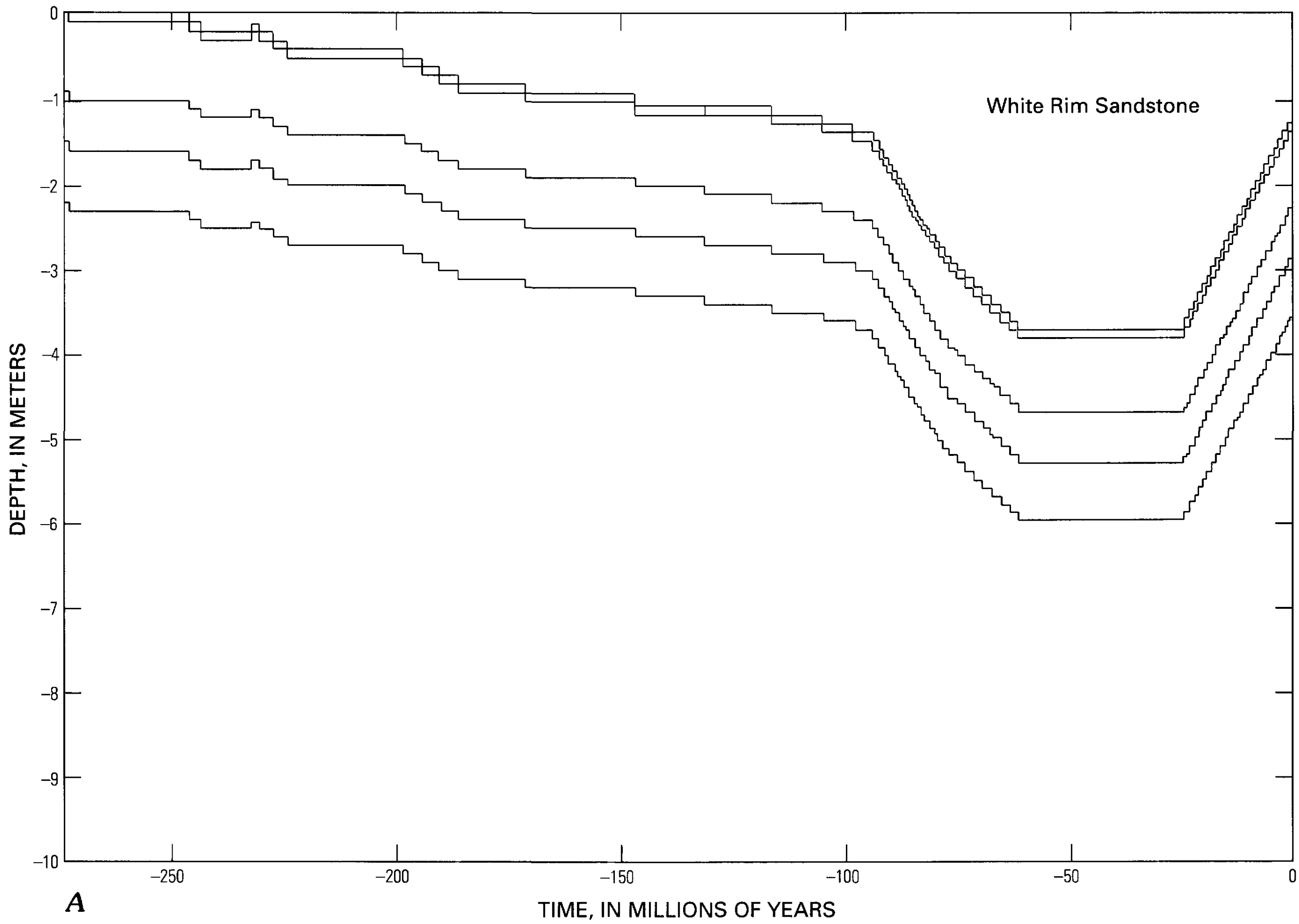

Figure 32 (above and following page). Burial history reconstructions of Lower Permian White Rim Sandstone in the Tar Sand triangle. *A*, Time versus depth. *B*, Time versus temperature (J. Huntoon, written commun., 1994).

been parallel with bedding because of the confinement of the White Rim Sandstone between semipermeable beds over much of its area of deposition.

These data constrain the time and direction of oil migration and, as a result, put constraints on potential source rocks; however, a source rock is also limited by the tremendous size of this deposit, unless more than one formation was the source. To form such a large accumulation, the source rock should have contained several percent of a hydrogen-rich kerogen, such as type I or II. For the source rock to have been any leaner would necessitate an unrealistically large volume of rock and (or) an unrealistic expulsion and migration efficiency.

Among the most promising source rocks are the Late Proterozoic Chuar Group, the Mississippian Delle Phosphatic Member of the Chainman Shale and equivalent formations, the Middle Pennsylvanian Paradox Formation of the Hermosa Group, the Lower Permian Phosphoria Formation and Kaibab Limestone, and the Lower Triassic Sinbad Limestone Member of the Lower and Middle(?) Triassic Moenkopi Formation. Because of the bouyancy of oil, migration almost certainly proceeded updip, and thus units stratigraphically above the White Rim are not candidates.

The source-rock potential of the Chuar Group is relatively unknown except for outcrops in the Grand Canyon area and in the Uinta Mountains. In northwestern Arizona, the Chuar is 5,120 ft (1,560 m) thick and has a total organic carbon (TOC) content of 9 weight percent in some algal carbonate rocks and mudstones (Palacas, 1992). The Chuar is an intriguing possibility as a source rock because it extends under the Paradox Basin, where it is now overmature and metamorphosed (Palacas and Reynolds, 1989). Oil would have had to migrate upward through faults and fractures either from the southwest or from directly under the Tar Sand triangle to reach the White Rim. Comparisons of carbon isotope, biomarker, and saturated hydrocarbon gas chromatogram data between tar sands in the White Rim Sandstone at Temple Mountain in the San Rafael Swell, oil at Circle Cliffs, and the tar in the Tar Sand triangle suggest that all came from the same source rock (Wenrich and Palacas, 1990). There are also some similarities between the oil in the Tar Sand triangle and the Chuar Group bitumens

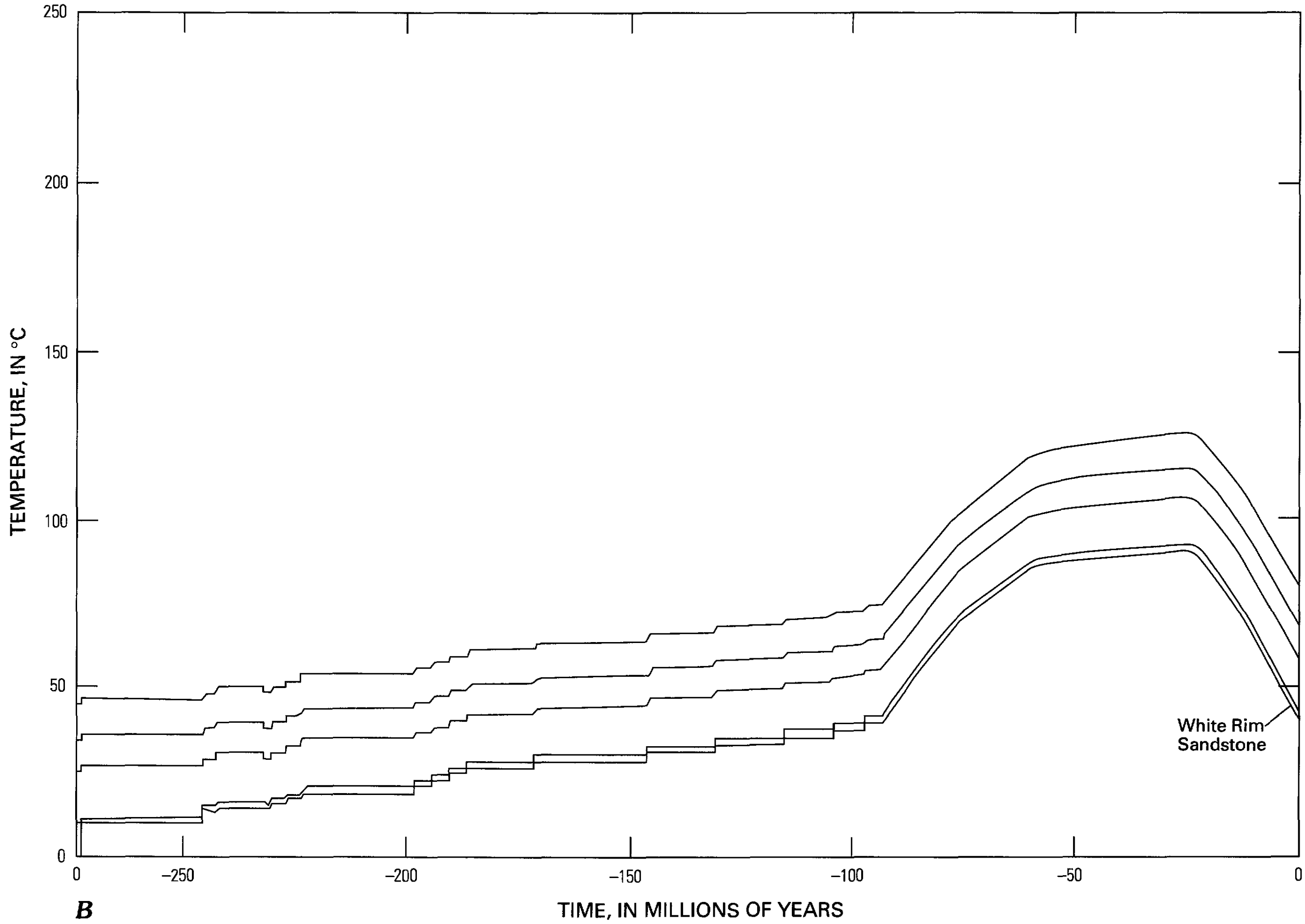

B

(Wenrich and Palacas, 1990). According to Sanford (in press), groundwater flow directions were favorable for northward flow from the middle late Campanian to the late Miocene (74–10 Ma). Using thicknesses of formations in various areas to the south of the Tar Sand triangle (Hintze, 1988) under which the Chuar Group may be present, the Chuar would probably have reached the oil window in the Jurassic; however, it is still in the oil window in the Grand Canyon region (J. Palacas, oral commun., 1993).

The Delle Phosphatic Member of the Chainman Shale and of the equivalent Woodman Formation is composed of micrite (80 percent) and phosphatic shale and contains from 3 to 8 weight percent total organic carbon in western Utah where it is immature to overmature (Poole and Claypool, 1984). Its high conodont alteration index suggests that the Delle has generated oil in the past (Sandberg and Gutschick, 1984). In western Utah, migration of oil from Cretaceous source rocks would have been assisted by thrust faulting during the Sevier orogeny in western Utah, which lasted from Aptian to early Tertiary time (Heller and others, 1986). Because of erosion, it is difficult to estimate when the Delle Phosphatic Member would have been mature in western Utah, but it probably was not mature until the early Tertiary.

The Paradox Formation of the Hermosa Group, which underlies the Permian section in the Paradox Basin, is an attractive source rock because it contains as much as 13 weight percent total organic carbon (Hite and others, 1984) and is near the Tar Sand triangle. Attempts at oil-source rock correlations based on geochemistry between it and the tar in the White Rim have, however, failed (J. Palacas, oral commun., 1993). Rough calculations using stratigraphic columns in Hintze (1988) show that the Paradox Formation probably began to generate oil in the Early Jurassic in the Moab area. Calculations are approximate because of the presence of salt, the unknown amount of erosion in the past, and variations in thickness of units in different parts of the basin.

The Phosphoria Formation in northwestern Utah has been suggested as a possible source rock for oil in the Middle and Upper Pennsylvanian and Lower Permian Tensleep Sandstone and Weber Sandstone and in the Lower Permian Park City Formation (Maughn, 1984). Mudstone, phosphorite, and dolomite of the Phosphoria average about 10 weight percent total organic carbon (Maughn, 1984). Because the White Rim is truncated by the Permian-Triassic unconformity to the southeast, it forms a favorable stratigraphic trap for fluids migrating from the northwest. Oil from southern

Idaho, southern Wyoming, or northern Utah would have had to migrate before Laramide faulting because hydrologic communication between the White Rim and source rocks to the northwest did not exist after that time (Sanford, in press). Based on burial reconstruction, oil is thought to have been generated in the Phosphoria Formation in early Mesozoic to Late Cretaceous time (Maughn, 1984).

The Kaibab Limestone consists of limestone, dolomite, sandstone, and evaporite facies. It is an attractive source rock because of its stratigraphic and geographic proximity to the White Rim; however, its total organic carbon content is generally low (<0.5 percent). Oil staining of the Kaibab in many areas of western Utah indicates that it has generated oil (B. Law, oral commun., 1993). Burial history estimates indicate that the Kaibab reached the oil window in Late Cretaceous to early Tertiary time west of the San Rafael Swell in western Utah.

The Sinbad Limestone Member of the Moenkopi Formation contains between 1 and 4 weight percent total organic carbon; however, it is not very thick (45–425 ft, 15–175 m) and thus probably could not have provided enough bitumen for such a large accumulation of oil. The Sinbad, similar to the Kaibab, probably reached the oil window in Late Cretaceous to early Tertiary time west of the San Rafael Swell.

All of these formations have been considered as source rocks for oil in the Tar Sand triangle. Most contain sufficient total organic carbon; they are all in favorable geographic and stratigraphic positions to meet the hydrologic requirements for delivering oil to the Tar Sand triangle; and they are known to have reached the oil window in the past. It is not inconceivable that combinations of these formations, or formations not discussed, were the source(s) of oil in the Tar Sand triangle.

OIL MIGRATION

The inverse relation between poikilotopic (early) calcite and oil (fig. 31) demonstrates that oil migration took place during and after calcite dissolution. Oil migration into the White Rim Sandstone in the Bullfrog area may have been earlier than in the Tar Sand triangle because in Bullfrog cores oil appears to fill primary pores. This apparent pore filling may, however, be an artifact of the preservation of primary porosity by the illite-smectite grain rims and the lack of alteration by meteoric water. The average homogenization temperature (83°C) of two-phase primary(?) inclusions in authigenic, oil-bearing dolomite fixes the minimum temperature of formation waters at the time of oil migration. The White Rim may have been buried deeply enough for indigeneous fluids to be in this temperature range, or a warm fluid may have migrated from below up into the cooler White Rim Sandstone when it was at a shallower depth. Because relatively impermeable siltstone and sandstone of the Organ Rock Shale underlie the White Rim in most of the area, hydrologic modeling indicates that fluids migrated laterally through the White Rim Sandstone and the overlying Permian-Triassic unconformity; therefore, this latter scenario is unlikely unless the waters moved upward along faults. There is little reported evidence for movement of hydrocarbons along faults in the area. As burial history reconstructions show, the formation temperature of the White Rim Sandstone at maximum burial was about 90°C, very close to the average homogenization temperature (83°C) of the fluid inclusions. The White Rim crossed the 83°C isotherm twice during its postdepositional history: once in the early Paleocene at approximately 11,726 ft (3,575 m) depth and again in the early Miocene at about 10,660 ft (3,250 m) depth (fig. 32). Because 83°C is so close to 90°C, they are considered to be essentially the same temperature.

Interpretation of textural relations between early calcite and oil and minus-cement porosity values of the calcite indicates that oil migration occurred after at least 300 m of burial. Some compaction also took place after dissolution of calcite cement and introduction of oil; therefore, oil is interpreted to have entered the sandstone after more burial, possibly as late as Cretaceous time. The presence of "dead" oil in the Island in the Sky District of Canyonlands National Park fixes the youngest time for migration as middle Tertiary because incision of the Green River began in Oligocene to Miocene time (Gardner, 1975). Lucchita (1973) concluded that the lower Colorado River did not exist until about 10.6 Ma, but he suggested that it may have captured a preexisting upper Colorado River. Based on the preceding data and interpretations, oil migration may have occurred between Cretaceous and middle Tertiary time.

Long-distance migration of hydrocarbons facilitated by tectonics has been proposed to explain long-distance migration of fluids in other areas (Oliver, 1986). Migration paths for oil were most likely to have been permeable sandstone, unconformity surfaces, and faults. To the west of the Tar Sand triangle, the White Rim and other upper Paleozoic units may have formed a relatively continuous aquifer all the way to Nevada before basin and range faulting in the Tertiary. Because subsurface flow in the White Rim Sandstone and adjacent aquifers was from west to east in Cretaceous to middle Tertiary time (Sanford, in press), hydrodynamic flow facilitated by tectonic forces during the Sevier orogeny could have provided the impetus for movement of large amounts of oil over long distances. Thrust sheets could have acted like giant "squeegees," pushing fluids ahead of them (Oliver, 1986). Stacking of large thrust plates may have locally doubled the geologic section, causing more rapid maturation of organic-rich rocks (Royse, 1993). West-east thrust faults also provided surfaces along which oil could migrate;

however, they could also have been barriers to fluid migration. After thrusting, these aquifers were probably too discontinuous due to basin and range faulting to transport oil for long distances.

CONCLUSIONS

A synthesis of fluid inclusion data, paragenesis of diagenetic alterations, and burial history reconstruction of the Lower Permian White Rim Sandstone in the Tar Sand triangle of southeastern Utah strongly favors oil migration near the time of deepest burial in Cretaceous to middle Tertiary time. Hydrology of the White Rim Sandstone suggests that fluid flow through it would have been mostly horizontal, and this conclusion suggests derivation of the oil from source rocks to the west. Because of the proposed long migration distance from some of the potential source rocks to the west, the driving force for secondary migration of oil may have been west-to-east thrusting during the Sevier orogeny (Early Cretaceous to early Tertiary). Most oil may have migrated along major, continuous surfaces such as faults and unconformities in addition to through permeable sandstones. Long-distance migration is typical of other giant accumulations of oil, such as in Venezuela or Alberta, that are in stratigraphic traps on the margins of basins.

The diagenetic and burial history data presented in this report constrain, for the first time, the timing of oil migration into the Tar Sand triangle. When these data are combined with results of ongoing studies of fission tracks in detrital apatite in the White Rim Sandstone and burial history modeling of potential source rocks, more conclusions may be drawn regarding the source of this giant accumulation of oil.

REFERENCES CITED

Baars, D.L., 1962, Permian System of Colorado Plateau: American Association of Petroleum Geologists Bulletin, v. 46, p. 149–218.

Baars, D.L., and Seager, W.R., 1970, Stratigraphic control of petroleum in White Rim Sandstone (Permian) in and near Canyonlands National Park, Utah: American Association of Petroleum Geologists Bulletin, v. 54, no. 5, p. 709–718.

Baars, D.L., and Stevenson, G.M., 1981, Tectonic evolution of the Paradox Basin, Utah and Colorado, *in* Wiegand, D.L., ed., Geology of the Paradox Basin: Rocky Mountain Association of Geologists Field Conference, p. 23–31.

Baker, A.A., 1946, Geology of the Green River Desert–Cataract Canyon region, Emery, Wayne, and Garfield Counties, Utah: U.S. Geological Survey Bulletin 951, 122 p.

Baker A.A., and Reeside, J.B., Jr., 1929, Correlation of the Permian of southern Utah, northern Arizona, northwestern New Mexico, and southwestern Colorado: American Association of Petroleum Geologists Bulletin, v. 13, no. 11, p. 1413–1448.

Bennett, P., and Siegel, D.I., 1987, Increased solubility of quartz in water due to complexing by organic compounds: Nature, v. 326, p. 684–686.

———1991, Silica-organic complexes and enhanced quartz dissolution in water by organic acids, *in* Miles, D.L., ed., Water-rock interaction: Water-Rock Interaction Conference, 6th, Proceedings; Rotterdam, Balkema, p. 69–72.

Bjorlykke, K., 1979, Diagenesis in Mesozoic sandstones from Spitsbergen and the North Sea—A comparison: Geologisches Rundschau, v. 68, p. 1152–1171.

Bodell, J.M., and Chapman, D.S., 1982, Heat flow in the north-central Colorado Plateau: Journal of Geophysical Research, v. 87, p. 2869–2884.

Campbell, J.A., and Ritzma, H.R., 1979, Geology and petroleum resources of the major oil-impregnated sandstone deposits of Utah: Utah Geological and Mineralogical Survey Special Publication 50, 24 p.

Chan, M.A., 1989, Erg margin of the Permian White Rim Sandstone, SE Utah: Sedimentology, v. 36, p. 235–251.

Clayton, R.N., 1959, Oxygen isotope fractionation in the system calcium carbonate-water: Journal of Chemical Physics, v. 30, p. 1246–1250.

Conybeare, C.E.B., 1967, Influence of compaction on stratigraphic analysis: Bulletin of Canadian Petroleum Geology, v. 15, p. 331–345.

Dana, G.F., Oliver, R.L., and Elliott, J.R., 1984, Geology and resources of the Tar Sand Triangle, southeastern Utah: U.S. Department of Energy Report DE–FC21–83FE60177, 50 p.

Dembicki, H., Jr., Anderson, M.J., and Diedrich, R.P., 1986, Oil-to-oil correlation in northwestern Colorado Plateau [abs.]: American Association of Petroleum Geologists Bulletin, v. 70, p. 1033.

Dickinson, W.W., 1991, Initial porosity in eolian sands—Revisited: Geological Society of America Abstracts with Programs, v. 23, p. A289–A290.

Dolson, J., and Henry, B., 1991, Physical expression of unconformity surfaces in the Shinarump Conglomerate (Tr-3 surface) and White Rim Sandstone (Late Permian and Tr-1 surfaces), Tar Triangle area, Utah, *in* Unconformity related hydrocarbon exploitation and accumulation in clastic and carbonate settings: Denver, Rocky Mountain Association of Geologists and the Exploration Geoscience Institute (Colorado School of Mines), Core Workshop, p. 151–158.

Dromgoole, E.L., and Walter, L.M., 1989, Effects of temperature and precipitation rate on incorporation of Fe^{2+} and Mn^{2+} into calcite: Geological Society of America Abstracts with Programs, v. 21, p. A18.

Dubiel, R.F., Parrish, J.R., Parrish, J.M., and Good, S.C., 1991, The Pangean megamonsoon—Evidence from the Upper Triassic Chinle Formation, Colorado Plateau: Palaios, v. 6, p. 347–370.

Dyman, T.S., Merewether, E.A., Molenaar, C.M., Cobban, W.A., Obradovich, J.D., and Weimer, R.J., and Bryant, W.A., 1994, Stratigraphic transects for Cretaceous rocks, Rocky Mountains and Great Plains regions, *in* Caputo, M.V., Peterson, J.A., and Franczyk, K.J., eds., Mesozoic systems of the Rocky Mountain region, USA: Denver, Rocky Mountain Section, Society for Sedimentary Geology, p. 365–392.

Folk, R.L., 1980, Petrology of sedimentary rocks: Austin, Hemphill, 184 p.

Fraser, D.G., Feltham, D., and Whiteman, M., 1989, High-resolution scanning proton microprobe studies of micron-scale trace element zoning in a secondary dolomite—Implications for studies of redox behaviour in dolomites: Sedimentary Geology, v. 65, p. 223–232.

Friedman, I., and O'Neil, J.R., 1977, Compilation of stable isotope fractionation factors of geochemical interest, *in* Fleischer, M., ed., Data of geochemistry, 6th ed.: U.S. Geological Survey Professional Paper 440–KK.

Gardner, T.W., 1975, The history of part of the Colorado River and its tributaries—An experimental study, *in* Canyonlands: Four Corners Geological Society Field Conference, 8th, Guidebook, p. 87–95.

Goldstein, R.H., and Reynolds, T.J., 1994, Systematics of fluid inclusions in diagenetic minerals: Society of Sedimentary Geology Short Course 31, 199 p.

Hansley, P.L., 1992, Diagenetic history of the Permian White Rim Sandstone Member, Cutler Formation, Tar Sand triangle, Paradox Basin: American Association of Petroleum Geologists, Annual Convention, 1992, Calgary, Abstracts, p. 51.

———1994, Paragenesis of a world-class tar sand deposit in the Permian White Rim Sandstone Member of the Cutler Formation, southeastern Utah: Rocky Mountain Section, Geological Society of America, Abstracts with Programs, v. 26, p. 16.

Heller, P.L., Bowdler, S.S., Chambers, H.P., Coogan, J.C., Hagen, E.S., Shuster, M.W., Lawton, T.F., and Winslow, N.S., 1986, Time of initial thrusting in the Sevier orogenic belt, Idaho-Wyoming and Utah: Geology, v. 14, p. 388–391.

Heylmun, E.B., 1958, Paleozoic stratigraphy and oil possibilities of the Kaiparowits region, Utah: American Association of Petroleum Geologists Bulletin, v. 42, p. 1781–1811.

Hintze, L.F., 1988, Geologic history of Utah: Brigham Young University Studies Special Publication 7, 203 p.

Hite, R.J., Anders, D.E., and Ging, T.G., 1984, Organic-rich source rocks of Pennsylvanian age in the Paradox basin of Utah and Colorado, *in* Woodward, J., Meissner, F.F., and Clayton, J.L., eds., Hydrocarbon source rocks of the greater Rocky Mountain region: Denver, Rocky Mountain Association of Geologists, p. 255–274.

Hoefs, J., 1987, Stable isotope geochemistry (3rd ed.): New York, Springer-Verlag, 241 p.

Hofmann, B.A., 1992, Organic matter associated with mineralized reduction spots in red beds, *in* Parnell, J., Kucha, H., and Landais, P., eds., Bitumens in ore deposits: New York, Springer-Verlag, p. 362–378.

Hunt, C.B., 1956, Cenozoic geology of the Colorado Plateau: U.S. Geological Survey Professional Paper, 279, 99 p.

Hunter, R.E., 1977, Basic types of stratification in small eolian dunes: Sedimentology, v. 24, p. 361–387.

Huntoon, J.E., 1985, Depositional environments and paleotopographic relief of the White Rim Sandstone (Permian) in the Elaterite basin, Canyonlands National Park and Glen Canyon National Recreation Area: Salt Lake City, University of Utah, M.S. thesis, 143 p.

Huntoon, J.E., and Chan, M.A., 1987, Marine origin of paleotopographic relief on eolian White Rim Sandstone (Permian), Elaterite Basin, Utah: American Association of Petroleum Geologists Bulletin, v. 71, p. 1035–1045.

Huntoon, J.E., Dolson, J., and Henry, B., in press, Seals and migration pathways in paleogeomorphically trapped petroleum occurrences—Permian White Rim Sandstone, tar-sand triangle area, Utah, *in* Dolson, J.C., Hendricks, M., Schanley, K., and Wescott, B., eds., Unconformity-related hydrocarbon accumulations and exploitation in clastic and carbonate settings: Denver, Rocky Mountain Association of Geologists, Field Conference, 1993, Guidebook.

Huntoon, J.E., Dolson, J., and Stanesco, J.E., 1994, Tectonic influence on development of the Permian-Triassic unconformity and basal Triassic strata, Paradox Basin, southeastern Utah, *in* Caputa, M.V., Peterson, J.A., and Franczyk, K.J., eds., Mesozoic systems of the Rocky Mountain region, USA: Denver, Rocky Mountain Section, Society of Sedimentary Geology, p. 109–132.

Huntoon, J.E., Dubiel, R.F., and Stanesco, J.D., 1994, Tectonic activity at the Permian-Triassic boundary and its infuence on deposition of basal Triassic strata, Paradox basin, southeastern Utah: Geological Society of America Abstracts with Programs, v. 26, no. 6, p. 19.

Huntoon, J.E., Hansley, P.L., and Palacas, J.G., 1994, Burial history modeling of potential source rocks for the Tar Sand triangle, southeastern Utah: Rocky Mountain Section, Geological Society of America, Abstracts with Programs, v. 26, p. 20.

Irwin, C.D., 1971, Stratigraphic analysis of Upper Permian and Lower Triassic strata in southern Utah: American Association of Petroleum Geologists Bulletin, v. 55, p. 1976–2007.

Johansen, S.J., 1988, Origins of upper Paleozoic quartzose sandstones, American southwest: Sedimentary Geology, v. 56, p. 153–166.

Kamola, D.L., and Chan, M.A., 1988, Coastal dune facies, Permian Cutler Formation (White Rim Sandstone), Capitol Reef National Park area, southern Utah: Sedimentary Geology, v. 56, p. 341–356.

Kamola, D.L., and Huntoon, J.E., 1994, Changes in rate of transgression across the Permian White Rim Sandstone, southern Utah: Journal of Sedimentary Research, v. B64, p. 202–210.

Keith, M.L., and Weber, J.N., 1964, Carbon and oxygen isotopic composition of selected limestones and fossils: Geochimica et Cosmochimica Acta, v. 28, p. 1787–1816.

Kerns, R., 1984, Utah tar sands: Survey Notes, v. 17, no. 4, p. 1–9.

Kharaka, Y.K., Law, L.M., Carothers, W.W., and Goerlitz, D.F., 1986, Role of organic species dissolved in formation waters from sedimentary basins in mineral diagenesis, *in* Gautier, D.L., ed., Roles of organic matter in sediment diagenesis: Society of Economic Paleontologists and Mineralogists Special Publication 38, p. 111–122.

Kinsman, D.J.J., 1966, Gypsum and anhydrite of Recent age, Trucial Coast, Persian Gulf, *in* Second Symposium on Salt: Northern Ohio Geological Society, v. 1, p. 302–326.

Kocurek, G., 1981, Significance of interdune deposits and bounding surfaces in aeolian dune sands: Sedimentology, v. 28, p. 753–780.

Longstaffe, F.J., 1983, Diagenesis 4, Stable isotope studies of diagenesis in clastic rocks: Geoscience Canada, v. 10, p. 43–58.

———1987, Stable isotopes of diagenetic processes, *in* Kyser, T.K., ed., Stable isotope geochemistry of low temperature processes: Saskatoon, Mineralogical Association of Canada, Short Course Handbook, v. 13, p. 187–257.

Lucchitta, I., 1972, Early history of the Colorado River in the Basin and Range Province: Geological Society of America Bulletin, v. 83, p. 1933–1948.

Machel, H.G., and Burton, E.E., 1991, Factors governing cathodoluminescence in calcite and dolomite, and their implications for studies of carbonate diagenesis, *in* Barker, C.E., and

Kopp, O.C., eds., Luminescence microscopy and spectoscopy—Qualitative and quantitative applications: Society of Economic Paleontologists and Mineralogists Short Course 25, p. 37–57.

Mack, G.H., 1978, The survivability of labile light-mineral grains in fluvial, aeolian and littoral marine environments—The Permian Cutler and Cedar Mesa Formations, Moab, Utah: Sedimentology, v. 25, p. 587–604.

Maughn, E.K., 1984, Geological setting and some geochemistry of petroleum source rocks in the Permian Phosphoria Formation, *in* Woodward, J., Meissner, F.F., and Clayton, J.L., eds., Hydrocarbon source rocks of the greater Rocky Mountain region: Denver, Rocky Mountain Association of Geologists, p. 281–294.

McKnight, E.T., 1940, Geology of area between Green and Colorado Rivers, Grand and San Juan Counties, Utah: U.S. Geological Survey Bulletin 908, 147 p.

Meybeck, M., 1979, Concentrations des eaux fluviales en elements majeurs et apports en solutions aux oceans: Revue de Geologie Dynamique et de Geographie Physique, v. 21, p. 215–246.

Oliver, J., 1986, Fluids expelled tectonically from orogenic belts—Their role in hydrocarbon migration and other geologic phenomena: Geology, v. 14, p. 99–102.

Palacas, J.G., 1992, Source-rock potential of Precambrian rocks in selected basins of the U.S., *in* Dyman, T.S., ed., Geologic controls and resource potential of natural gas in deep sedimentary basins in the United States: Final Report for the Gas Research Institute, p. 161–172.

Palacas, J.G., and Reynolds, M.W., 1989, Potential petroleum source rocks in the Late Proterozoic Chuar Group, Grand Canyon, Arizona, *in* Carter, L.M.H., ed., U.S. Geological Survey Research on Energy Resources–1988, Program and Abstracts: U.S. Geological Survey Circular 1025, p. 49–50.

Paquette, J., and Reeder, R.J., 1990, New type of compositional zoning in calcite—Insights into crystal-growth mechanisms: Geology, v. 18, p. 1244–1247.

Phillips, M., 1975, Cane Creek mine solution mining project, Moab potash operations, Texasgulf, Inc., *in* Fassett, J.E., and Wengerd, S.A., eds., Canyonlands country: Four Corner Geological Society Guidebook, p. 261.

Poole, F.G., 1962, Wind directions in late Paleozoic to middle Mesozoic time on the Colorado Plateau: U.S. Geological Survey Professional Paper 450–D, p. 147–151.

Poole, F.G., and Claypool, G.E., 1984, Petroleum source-rock potential and crude-oil correlation in the Great Basin, *in* Woodward, J., Meissner, F.F., and Clayton, J.L., eds., Hydrocarbon source rocks of the greater Rocky Mountain region: Denver, Rocky Mountain Association of Geologists, p. 179–227.

Potocki, D.J., 1989, The influence of deep meteoric invasion on the reservoir quality of Cretaceous sandstones in the Mackenzie Delta, Canada, *in* Miles, D.L., ed., Water-rock interaction: International Symposium on Water-Rock Interaction, 6th, Proceedings; Rotterdam, Balkema, p. 561–564.

Reeder, R.J., and Prosky, J.L., 1986, Compositional sector zoning in dolomite: Journal of Sedimentary Petrology, v. 56, p. 237–247.

Ritzma, H.R., 1979, Oil-impregnated rock deposits of Utah: Utah Geological and Mineral Survey Map 47, 1:1,000,000, 2 sheets.

Rock-Color Chart Committee, 1948, Rock-color chart: Boulder, Geological Society of America, 8 p.

Royce, F., Jr., 1993, Case of the phantom foredeep—Early Cretaceous in west-central Utah: Geology, v. 21, p. 133–136.

Sandberg, C.A., and Gutschick, R.C., 1984, Distribution, microfauna, and source-rock potential of Mississippian Delle Phosphatic Member of Woodman Formation and equivalents, Utah and adjacent states, *in* Woodward, J., Meissner, F.F., and Clayton, J.L., eds., Hydrocarbon source rocks of the greater Rocky Mountain region: Denver, Rocky Mountain Association of Geologists, p. 135–159.

Sanford, R.F., in press, Ground-water flow and migration of hydrocarbons to the Lower Permian White Rim Sandstone, Tar Sand triangle, southeast Utah: U.S. Geological Survey Bulletin 2000–J.

Schenk, C.J., 1983, Textural and structural characteristics of some experimentally formed eolian strata, *in* Brookfield, M.E., and Ahlbrandt, T.S., eds., Eolian sediments and processes: Developments in Sedimentology, v. 38, p. 41–49.

Scott, G.L., 1965, Heavy mineral evidence for source of some Permian quartzose sandstones, Colorado Plateau: Journal of Sedimentary Petrology, v. 35, p. 391–400.

Spencer, C.W., 1975, Petroleum geology of east-central Utah and suggested approaches to exploration: Four Corners Geological Society Field Conference, Canyonlands, 8th, Guidebook, p. 263–275.

Steele, B.A., 1987, Depositional environments of the White Rim Sandstone Member of the Permian Cutler Formation, Canyonlands National Park, Utah: U.S. Geological Survey Bulletin 1592, 20 p.

Steele-Mallory, B.A., 1981, The depositional environment and petrology of the White Rim Sandstone Member of the Permian Cutler Formation, Canyonlands National Park, Utah: Golden, Colorado School of Mines, M.S. thesis, T–2436, 121 p.

Surdam, R.C., Jiao, Z.S., and MacGowan, D.B., 1993, Redox reactions involving hydrocarbons and mineral oxidants—A mechanism for significant porosity enhancement in sandstones: American Association of Petroleum Geologists Bulletin, v. 77, p. 1509–1518.

Tissot, B.P., and Welte, D.H., 1984, Petroleum formation and occurrence (2nd ed.), New York, Springer-Verlag, 699 p.

Tubbs, R.E., Jr., 1989, Depositional history of the White Rim Sandstone, Wayne and Garfield Counties, Utah: The Mountain Geologist, v. 26, no. 4, p. 101–112.

Van der Plas, L., and Tobi, A.C., 1965, A chart for judging the reliability of point counting results: American Journal of Science, v. 263, p. 87–90.

Walker, R.G., and Middleton, G.V., 1981, Facies models 4—Eolian sands, *in* Walker, R.G., ed., Facies models: Toronto, Geological Association of Canada, p. 33–41.

Wenrich, K.J., and Palacas, J.G., 1990, Organic matter and uranium in solution—Collapse breccia pipes of northern Arizona and San Rafael Swell, Utah: U.S. Geological Survey Circular 1069, p. 36–50.Werner, W.G., 1974, Petrology of the Cutler Formation (Pennsylvanian-Permian) near Gateway, Colorado, and Fisher Towers, Utah: Journal of Sedimentary Petrology, v. 44, p. 292–298.

Werner, W.G., 1974, Petrology of the Cutler Formation (Pennsylvanian-Permian) near Gateway, Colorado, and Fisher Towers, Utah: Journal of Sedimentary Petrology, v. 44, p. 292–298.

Wogelius, R.A., Fraser, D.G., Feltham, D.J., and Whiteman, M.I., 1992, Trace element zoning in dolomite—Proton microprobe data and thermodynamic constraints on fluid compositions: Geochimica et Cosmochimica Acta, v. 56, p. 319–334.

APPENDIX—DESCRIPTION OF CORE

Appendix table 1. Description of TST2 core.
[Color from Rock-Color Chart Committee (1948)]

Depth below surface (feet)	Color	Grain size	Bedding	Description
1,415–1,417	10YR 3/2	Medium	Massive(?)	12.5-in. calcite nodule; top is broken.
1,417–1,418.2	10YR 2/2 to 10YR 4/2	Upper fine	Tabular-planar crossbedding	Alternating very dark (oil saturated) and light beds containing sparse calcite blebs.
1,418.2–1,426	10YR 4/2	Upper fine to medium	Tabular-planar crossbedding	Not as saturated as above.
1,426–1,428.2	10YR 4/2	Fine to medium	High-angle crossbedding	Thin, medium-grained sandstone beds appear darker due to dissolution.
1,428.2–1,428.4	10YR 2/2 to 10YR 4/2	Fine to medium	Low-angle crossbedding	Medium-grained sandstone is more saturated.
1,428.4–1,429	10YR 4/2	Lower fine to upper fine	High-angle crossbedding	Rippled from 1,428 to 1,428.5 ft.
1,429.0–1,430 (1,429.7–1,430 missing)	10YR 3/2 to 10YR 2/2	Fine	Tabular-planar; almost no crossbedding	Bioturbated(?). Some low-angle crossbedding; alternating beds of lower fine to upper fine (occasionally lower medium); dissolution vugs abundant; white calcite blebs; a few 0.25-in. beds of very fine dark sandstone (10YR 3/2) that comprises well-rounded grains and is not as well sorted.
1,430–1,431.5	10YR 3/2	Lower fine	Massive	Broken up at base.
1,431.5–1,441.5	10YR 4/2	Fine	High-angle crossbedding in some places	Broken-up core; half large-, half small-diameter core.
1,441.5–1,444.5	10YR 4/2	Upper fine	Low-angle crossbedding	Sparse 1/16-in. white calcite-cemented beds; at 1,443.3 ft black tabular-planar sandstone is unconformable on high-angle crossbedded sandstone below; well sorted.
1,444.5–1,444.8		Upper fine to lower medium	Tabular-planar crossbedding	Gray calcareous beds.
1,444.8–1,447	10YR 4/2 to 10YR 2/2 to 5YR 2/2	Upper fine to lower medium	High- to low-angle crossbedding	Darker in coarser units and lower angle crossbeds; black beds are upper fine grained.
1,447–1,448	10YR 4/2	Lower fine to fine	High-angle crossbedding	Well sorted.
1,448–1,449.5	N8 to 10YR 4/3	Lower fine	Tabular-planar crossbedding	Mottled calcite cement; “cauliflower” pattern.
1,449.5–1,450.3	5YR 6/1			Calcite nodule (after gypsum or anhydrite).
1,450.3–1,455	10 YR 3/2	Fine	Low- to high-angle crossbedding at base	
Missing				
1,460.6–1,463.6	10YR 3/2	Upper fine	High-angle crossbedding	Oil saturated and calcite cemented.
1,463.6–1,466.8	10YR 3/2			Same as above; broken up.
1466.8–1467	N8	Lower fine to fine		Calcite-cemented areas.
1,467–1,467.4				Mostly calcite; black at top.
1,467.4–1,474	N7	Very fine	High-angle crossbedding	Oil-saturated and calcitic layers; oil saturated especially in second foot; lower 2.5 ft is mostly calcite.
1,474–1,475	10YR 3/2	Very fine to lower fine	High-angle crossbedding	Oil saturated with some calcite blebs; grades into “cauliflower” calcite.
1,475–1,475.8	N6 to N5	Very fine	High-angle crossbedding	Calcite cemented; trace oil.
1,475.8–1,476.8	10YR 4/2	Fine	High-angle crossbedding over tabular-planar crossbedding	High-angle crossbeds are calcite cemented; tabular-planar beds are oil saturated.
1,476.8–1,478.2	10YR 3/2	Upper fine	Moderate-angle crossbedding	Uniform; sparse calcite; well sorted.
1,478.2–1,478.6	10YR 4/2 to 5Y 6/1 (insides of white blebs)	Upper fine		“Cauliflower”texture (calcite cemented).
1,478.6–1,480.2	10YR 4/2	Upper fine	Tabular-planar crossbedding	Pieces; calcite cemented.
1,480.2–1,483.6	10YR 4/2	Upper fine		Pieces.
1,483.6–1,489.4	10YR 3/2	Upper fine	Low-angle crossbedding	Sparse calcite-cemented areas.

1,489.4–1,496	10YR 3/2 to 10YR 2/2	Upper fine to lower medium	High-angle crossbedding	Oil saturated; quartz overgrowths(?)
1,496–1,498	10YR 4/2	Fine	High-angle crossbedding	Oil saturated
1,498–1,499.2	Broken(?)			
1,499.2–1,500.8	10YR 4/2	Upper fine		Sparse calcite cement; some black laminae.
1,500.8–1,503.8	10YR 3/2	Fine to upper fine	High-angle crossbedding	<10 percent black beds.
1,503.8–1,505.8	10YR 3/2 to N8	Upper fine; medium when black	Low-angle crossbedding	Oil saturated.
1,505.8–1,508.5	N8	Upper fine; medium when black	Rippled(?)	Oil saturated.
1,508.5–1,511	10YR 4/2	Fine	Low-angle	Calcite cement at base.
1,511–1,519.9	10YR 4/2	Fine	Moderate-high-angle crossbedding	Sparse, thin saturated beds; pale calcite blebs in bottom 2.4 ft.
1,519.9–1,528.9	10YR 4/2	Fine to upper fine	High-angle crossbedding	Pale mottled to about 1,520.5 ft; alternating light- and dark-brown near base.
1,528.9–1,531	10YR 3/2 and 2/2	Upper fine	High-angle crossbedding	
1,531–1,533	Sharp color break; 10YR 2/2	Upper fine	Rippled(?)	Complex bedding.
1,533–1,534.5	10YR 2/2	Upper very fine to lower fine	High-angle crossbedding	Fines upward; rippled.
1,534.5–1,537	5YR 2/2	Lower fine to lower medium	High-angle crossbedding	Color depends on saturation; crossbeds alternate with rippled beds.
1,537–1,538.8	10YR 4/2	Fine	Tabular-planar crossbedding	Slightly rippled.
1,538.8–1,540.3	5YR 3/2; 5Y 8/1 bands	Fine	Tabular-planar crossbedding	Large colloform pyrite (1.5 in. by 2 in.).
1,540.3–1,547.5	Missing			
1,547.5–1,553	5YR 2/1 to 10YR 2/2	Medium	Low-angle crossbedding and tabular-planar crossbedding	Chert pebbles; saturated; poorly sorted; rippled.
1,553–1,557	5YR 2/1	Fine	High-angle crossbedding	Vuggy porosity; pyrite 1,551.5–1,557 ft ; color change from brown to light brown at crossbedding change; large cherts at 1,550 ft.
1,557–1,557.3	N8	Fine	Low-angle crossbedding	
1,557.3–1,568.1	10YR 3/2	Fine	High-angle crossbedding	Change in crossbedding direction at 1,558 ft; 1,557–1,558 ft, moderate angle (15°); 1,558–1,558.3 ft, rippled, horizontal; 1,558.3–1,559 ft, high-angle crossbeds downward to lower angle crossbeds at base; well sorte.
1,568.1–1,570.1	N8	Upper fine	High-angle crossbedding	Heavily mottled with calcite and oil.
1,570.1–1,571.1	5YR 2/1	Upper fine	Low-angle crossbedding	Less mottling than overlying interval; change in crossbedding direction.
1,571.1–1,573.6	N8 to 10YR 3/2	Upper fine	Tabular-planar crossbedding to low-angle crossbedding	Alternating black and less saturated beds (more porous); some white and brown calcareous layers; moderate sorting; rippled.
1,573.6–1,574.5	10YR to 5YR 2/2	Upper fine to lower medium	Tabular-planar, rippled crossbedding	Rippled.
1,574.5–1,575	10YR 2/2	Very fine	Moderate-angle crossbedding	
1,575–1,576.5	10YR 4/2	Fine	High-angle crossbedding	Alternating black and brown lower 6 in.
1,576.5–1,577.5	N8	Fine	High-angle crossbedding	
1,577.5–1,578.8	5YR 2/2 to10YR 8/2	Lower medium to medium	Tabular planer; low-angle crossbedding	Interdune lag(?); white calcite-cemented beds; rippled.
1,578.8–1,579.2	5YR 4/2	Fine	Low-angle crossbedding	
1,579.2–1,579.9	10YR 2/2	Fine	Low-angle crossbedding	
1,579.9–1,580.9	10YR 2/2	Fine	Tabular-planar crossbedding	

Appendix table 2. Description of TST3 core.
[Color from Rock-Color Chart Committee (1948)]

Depth below surface (feet)	Color	Grain size	Bedding	Description
1,412–1,413	5YR 2/1 to N8	Fine	High-angle crossbedding; tabular-planar crossbedding near base	Sparse oil stain; a few calcite-cemented beds.
1,413–1,415	N3 to N8	Fine	Tabular-planar crossbedding to low-angle crossbedding	Saturated; a few lighter beds are calcite cemented; some mottling.
1,415–1,415.6	5YR 3/1 to 5Y 7/1	Very fine	Crossbedded	Calcareous; oil stained.
1,415.6–1,417.8	N8 to N9	Fine	High- to low-angle crossbedding at base	Very white; sparse oil mottling at top; fines upward; lower part of interval is better sorted.
1,417.8–1,418	N8	Very fine	Rippled	Calcareous.
1,418–1,418.4	10YR 4/2	Fine	Tabular-planar crossbedding; wavy	Mottled; oil stain.
1,418.4–1,419	N8		Fine	Low-angle crossbedding.
1,419–1,419.4	10YR 8/2	Fine	Low-angle crossbedding	Calcareous; mottled.
1,419.4–1,421	10YR4/2	Fine	Tabular-planar crossbedding to low-angle crossbedding at base	Oil saturated; sparse calcite mottling at base.
1,421–1,425	10YR 4/2	Fine	Low-angle crossbedding	Calcite mottling (N8); heavy-mineral laminae.
1,425–1,426	10YR 4/2	Very fine	Low-angle crossbedding	Oil saturated.
1,426–1,431	10YR 3/2	Fine	Low-angle crossbedding	Oil saturated; finer at base; climbing ripples(?).
1,431–1,431.4	10YR 4/2	Fine to medium	Rippled	Lag.
1,431.4–1,433	10YR 4/2	Fine	Moderate- to high-angle crossbedding	Oil saturated.
1,433–1,434	10YR 3/2	Very fine to fine at base	High-angle crossbedding	Oil saturated.
1,434–1,452	Missing			
1,452–1,454.5	10YR 4/2	Medium to fine toward base	Moderate-angle crossbedding	Oil saturated; pyrite at 1,453 ft; minor calcite cement.
1,454.5–1,456	10YR 4/2	Fine	High-angle crossbedding	Oil saturated.
1,456–1,459	10YR 4/2	Fine	Tabular-planar crossbedding	Rippled; oil saturated.
1,459–1,463	10YR 4/2	Fine	Low-angle to tabular-planar crossbedding	Mottled with calcite cement; oil.
1,463–1,466	10YR 3/2	Fine	Low-angle crossbedding	Oil saturated.
1,466–1,469	10YR 4 /2	Fine	Low-angle crossbedding	Oil; fines slightly downward.
1,469–1,470.6	5YR 3/2	Fine	Low-angle crossbedding	Oil saturated; pieces.
1,470.6–1,471.8	5YR 2/1	Fine	Low-angle crossbedding	Oil saturated.
1,471.8–1,473	10YR 4/2	Fine	Indistinct	Some very fine and medium grains.
1,473–1,478	10YR 4/2	Fine	High-angle crossbedding	Calcareous; some coarser grains; oil stained.
1,478–1,481	5YR 3/2 and 2/2	Fine	Moderate- to low-angle crossbedding	Oil saturated; pieces.

Appendix table 3. Description of TST4 core.
[Color from Rock-Color Chart Committee (1948)]

Depth below surface (feet)	Color	Grain size	Bedding	Description
1,402–1,410	10YR 4/2	Fine to medium at base	Moderate- to high-angle crossbedding	Uniform.
1,410–1,412.6	10YR 4/2	Upper very fine	Low-angle to tabular-planar crossbedding	Rippled(?).

1,412.6–1,415.7	10YR 4/2	Upper very fine	High-angle crossbedding	Pyrite.
1,415.7–1,415.9	5YR 4/4	Upper very fine	High-angle crossbedding	
1,415.9–1,417.1	10YR 4/2	Upper fine	Low-angle crossbedding to tabular-planar crossbedding	Black laminae; pyrite rippled.
1,417.1–1,418	N1 to 10YR 4/2	Upper fine at top to medium at base	Low-angle crossbedding	Calcareous intervals.
1,418–1,419.7	N1	Upper very fine at top to fine at base	Low-angle crossbedding	Oil saturated; mottled with calcite cement; pyrite; rippled at base.
1,419.7–1,422.3	N1 to N7	Very fine	Rippled	Medium-grained lag at 1,420.5 ft.
1,422.3–1,424	N1 to 10YR 4/2	Medium	Low-angle crossbedding	Rippled; colors are interbedded; calcareous.
1,424–1,430	5YR 3/2	Upper very fine	Rippled	Calcareous; rippled.
1,430–1,434	10YR 4/2 to N8	Very fine	Low-angle crossbedding	Rippled; calcite cement in less saturated areas; pyrite nodule (0.25 in.) at 1,433.4 ft.
1,434–1,444	Missing			
1,444–1,450	5YR 2/2 to N8	Upper medium	Low-angle crossbedding	Alternating black and brown beds.
1,450–1,453.5	10YR 4/2	Upper very fine to upper medium	High- to low-angle crossbedding; tabular-planar crossbedding at base	
1,453.5–1,455.5	5YR 2/2	Upper medium to very fine at base	Tabular-planar crossbedding	Rippled.
1,455.5–1,460.5	10YR 4/2	Very fine	None	No structures visible.
1,460.5–1,464	Core loss			
1,464–1,471.6	10YR 4/2	Very fine to fine	Moderate-angle crossbedding	Mostly fine; interspersed lags; sparsely mottled white.
1,471.6–1,472.5	N8	Medium	Moderate-angle crossbedding	Oil-saturated beds alternating with less saturated bands.
1,472.5–1,476.9	N8 to 10YR 6/2	Medium	Low-angle crossbedding	Sparse calcite and pyrite.
1,476.9–1,477.7	10YR 5/2	Upper fine	Low-angle crossbedding to tabular-planar crossbedding	Less oil saturation.
1,480–1,483.6	5YR 2/1	Medium	Low-angle crossbedding	Pyrite near base.
1,483.6–1,486	10YR 5/2	Fine	Tabular-planar crossbedding to low-angle crossbedding	Pyrite.
1,477.7–1,480	5YR 3/2	Coarse	Low-angle crossbedding	
1,486–1,490	10YR 4/2	Fine	Tabular-planar crossbedding to low-angle crossbedding	A few white calcite-cemented and black saturated beds.
1,490–1,496	N1	Fine-medium	Tabular-planar to low-angle crossbedding	
1,496–1,512.9	10YR 4/2 to 2/2	Upper medium to fine	Tabular-planar crossbedding to low-angle crossbedding	Local areas of calcite cement; fines downward.
1,512.9–1,514.3	10YR 4/2	Medium	None visible	
1,514.3–1,516.8	N1	Upper fine	Low-angle crossbedding	Oil saturated.
1,516.8–1,520.3	10YR 4/2 to N1	Fine	Moderate- to high-angle crossbedding	Brown to black to white; variable depending on saturation.
1,520.3–1,521	N8 to N9	Upper medium	Moderate-angle to tabular	Oil-saturated planar crossbedding.
1,521–1,522	10YR 4/2	Upper medium	Low-angle crossbedding	

Appendix table 4. Description of Bullfrog No. 1 core.
[Color from Rock-Color Chart Committee (1948). Core in all boxes is in pieces, so depths are approximate; most oil saturation ends at 3,020 ft; grain size changes dramatically over a distance of a few inches]

Depth below surface (feet)	Color	Grain size	Bedding	Description
2,972–2,976	N1	Fine	Low-angle crossbedding	Oil saturated; a few white calcite-cemented beds.
2,976–2,980	5YR 2/1	Upper fine to lower medium	Low-angle crossbedding	Some white mottled pieces.
2,980–2,986	5YR 2/1	Fine	Low-angle crossbedding	Spots of kaolinite; coarse grains on crossbeds; rippled; visible porosity.
2,986–2,991	N1	Fine to lower medium	High-angle crossbedding	Pieces; oil saturated.
2,991–2,996	N1	Medium to coarse	High-angle crossbedding	Oil saturated.
2,996–3,001	N1 to 10YR 4/2	Fine	Low- to high-angle crossbedding	Mostly white; noncalcareous.
3,001–3,005	N1 to 10YR 4/2	Very fine to fine	High angle crossbedding	Mottled with kaolinite.
3,005–3,008	N1 to 10YR 4/2	Fine	High angle crossbedding	Alternating saturated and unsaturated beds.
3,006–3,016	10YR 4/2	Very fine to lower medium	High-angle crossbedding	Some saturated beds.
3,016–3,021	10YR 6/2 to N6	Fine to coarse	Low-angle crossbedding to tabular-planar crossbedding	Alternating saturated and unsaturated beds; pyrite; calcareous.
3,021–3,026	10YR 6/2 to N6	Fine to medium	Low-angle crossbedding	Rippled.
3,026–3,032	10YR 6/2 to N6	Very fine to fine	High-angle crossbedding to tabular-planar crossbedding	Rippled.
3,032–3,037	10YR 6/2	Very fine to fine	Moderate- to high-angle crossbedding	Calcareous; a few oil-saturated beds.
3,037–3,042	10YR 6/2	Fine	High-angle crossbedding	A few oil-saturated beds.

Appendix table 5. Description of Muley Creek State No. 36–33 core.
[Color from Rock-Color Chart Committee (1948)]

Depth below surface (feet)	Color	Grain size	Bedding	Description
4,022–4,025.2	10YR 4/2 to 5YR 5/2	Very fine	Wavy	Variably oil saturated; calcareous.
4,025.2–4,028.4	10YR 4/2	Very fine	Wavy	Dolomitic(?).
4,028.4–4,031.7	10YR 4/2	Very fine	Wavy	Algal(?); dolomitic; vuggy
4,031.7–4,035.3	10YR 4/2	Very fine	Wavy	Pyritic laminae; organic; dolomitic.
4,035.3–4,038.2	10YR 4/2 to 5B 9/1	Very fine	Wavy	Algal; calcareous; oil saturated in lower 1.5 ft; top half is white and lower half is brown.
4,038.2–4,044.4	10YR 2/2	Very fine	Vuggy	Oil saturated; mottled with some calcareous areas.
4,044.4–4,048	10YR 4/2	Very fine to fine	Deformed	White and brown mottling.
4,048–4,051.5	5Y 2/2 to N1	Fine	High-angle crossbedding	Oil saturated; rippled at top.
4,051.5–4,055.1	10YR 4/2	Fine	High-angle crossbedding	Oil saturated.
4,055.1–4,058.3	10YR 4/2	Fine	High-angle crossbedding at top	Wavy; mottled white/brown.
4,058.3–4,061.4	10YR 4/2 to N1	Fine	Deformed	Oil saturated to mottled; wispy organic(?) matter at base.
4,061.4–4,064.6	N8	Fine	Wavy	Mottled with oil staining; wispy organic(?) laminae.
4,064.6–4,068.2	10YR 8/2	Fine	Wavy	Mottled with oil staining.
4,068.2–4,071.5	10YR 8/2 to N8	Fine to very fine	Wavy	Poorly sorted.
4,071.5–4,075	10YR 8/2	Fine to upper medium	Wavy; rippled	Greenish pyritic laminae; wispy organic(?) matter.
4,075–4,084	10YR 8/2	Fine to coarse	Tabular-planar crossbedding; wavy	Rippled.

Appendix table 6. Description of East Muley Creek No. 1 core.
[Color from Rock-Color Chart Committee (1948)]

Depth below surface (feet)	Color	Grain size	Bedding	Description
2,886–2,892	5YR 6/2 to 10YR 7/2	Fine	High-angle crossbedding	Alternating thin gray and pink beds.
2,892–2,904	5YR 6/2 to 10YR 7/2	Fine to coarse	High-angle crossbedding	Same as above.
2,904–2,910	5YR 6/2 to 10YR 7/2	Fine to medium	Rippled	
2,910–2,916	5R 5/2	Fine	Rippled; low-angle crossbedding	
2,916–2,922	10R 6/2 to 5R 8/2 to N5 and N6	Fine to coarse	Crossbedded; rippled	Kaolinite.
2,922–2,929	10R 6/2 to 5R 8/2 to N5 and N6	Fine	High-angle tabular-planar crossbedding	
2,929–2,935	10R 4/2 to 6/2	Fine to medium	Tabular-planar crossbedding to low-angle crossbedding	
2,935–2,943	10R 4/2	Fine	Tabular-planar crossbedding to high-angle crossbedding	Dolomite cement.
2,943–2,950	10R 4/2 to 10YR 8/2	Fine	Tabular-planar crossbedding	Rippled; mottled; gray cement.
2,950–2,956	10YR 8/2 to 5YR 6/2	Fine to medium	Tabular-planar crossbedding to high-angle crossbedding	
2,956–2,959	10R 6/2	Fine to medium	High-angle crossbedding	Gray beds at top; heavy-mineral laminae at 2,957 ft.

☆U.S. GOVERNMENT PRINTING OFFICE: 1995-673-046/86126